Molecular evidence for pre-chordate origins of ovarian cell types and neuroendocrine control of reproduction

Periklis Paganos[1], Carsten Wolff[1], Danila Voronov[2], S. Zachary Swartz[1*]

[1] Marine Biological Laboratory, 7 MBL Street, Woods Hole, Massachusetts, 02543, United States of America

[2] Max Planck Institute for Evolutionary Biology, August-Thienemann-Straße 2, 24306 Plön, Germany

*correspondence: zswartz@mbl.edu

Abstract

Sexual reproduction in animals requires the development of oocytes, or egg cells. This process, termed oogenesis, requires complex interactions amongst germline and somatic cell types in the ovary. How did these cell types and their signaling interactions evolve? Here we use the sea star *Patiria miniata* as a non-chordate deuterostome representative to define the ovarian cell type toolkit in echinoderms. Sea stars continuously produce millions of new oocytes throughout their lifespan, making them a practical system to understand the mechanisms that drive oogenesis from a biomedical and evolutionary perspective. We performed scRNA-seq combined with high-resolution 3D-imaging to reveal the ovarian cell types and their spatial organization. Our data support the presence of actively dividing oogonial stem cells and granulosa-like and theca-like cells, which display similarities and possible homology with their mammalian counterparts. Lastly, our data support the existence of an endocrine signaling system between oogonial stem cells and intrinsic ovarian neurons with striking similarities to the vertebrate hypothalamic-pituitary-gonadal axis. Overall, this study provides molecular evidence supporting the possible pre-chordate origins of conserved ovarian cell types, and the presence of an intrinsic neuroendocrine system which potentially controls oogenesis and predates the formation of the hypothalamic-pituitary-gonadal axis in vertebrates.

Keywords: sea star, single cell transcriptomics, oogenesis, oogonial stem cells, HPG-axis.

Introduction

Oogenesis is essential for the propagation of most animal species. This process takes place within the ovary, where somatic and germ cells interact to form a fundamental reproductive unit: the follicle (1). Diverse ovarian cell types underlie these interactions and define the reproductive potential of the organism. For instance, somatic follicle cells, also referred to as granulosa in mammals, are in direct contact with developing oocytes and provide signals and metabolic support to regulate growth and meiotic arrest. Mammalian theca cells in the outer layers of the follicles have a key role in steroid hormone production, nutrient delivery to the follicle through the vasculature, and regulating granulosa cell function (2). In vertebrates, the hypothalamic-pituitary gland-gonadal (HPG) axis provides hormonal cues from the central nervous system essential for proper germ cell growth, maturation, and ovulation (3).

Many germ line processes are broadly conserved, but different organisms have diverse reproductive potentials due to the presence or absence of specific cell types or states. For instance, the mammalian oocyte reserve is established during embryogenesis, during which germ cells are limited to either entering meiosis, generating oocytes that remain arrested until puberty, or undergoing apoptosis (4). This limited number of oocytes shows signs of developmental decline with age in both mice and humans (5). Other animals such as the fruit fly instead produce oocytes throughout their lifespans due to a well-defined germ line stem cell niche that persists through adulthood (6). However, the mechanisms controlling oogenesis and the establishment of reproductive potential in other metazoans remain less understood. Moreover, numerous evo-devo studies have identified conserved genes expressed in germ line cells (7), but much less is known about the evolutionary history of the other somatic cell types within ovaries.

Echinoderms are non-chordate deuterostomes (8), a phylogenetic position informative for both vertebrates and other invertebrates, thus making them a valuable experimental

63 system for addressing questions about the deep evolution of reproductive cell types (**Fig.**
64 **1A**). Echinoderms including sea stars continuously produce millions of oocytes that
65 develop into optically transparent embryos and larvae, and have documented lifespans
66 that can exceed a century (9). However, while echinoderms have been extensively used
67 to study fertilization, gene regulation, and embryogenesis due to the abundance of eggs
68 they provide, we still lack a mechanistic understanding for how they achieve this
69 remarkable reproductive output (10,11).
70
71 In this work, we asked how the reproductive potential of the sea star *Patiria miniata* is
72 controlled, and whether sea star ovarian cell types are conserved with distantly related
73 animals. Using high-resolution microscopy and single cell RNA sequencing (scRNA-seq),
74 we defined the cellular organization of the sea star ovary, determined its cell types, and
75 explored their evolutionary relationships with other animals. We found the ovary to consist
76 of epithelial cells, immune cells, neurons, oocytes, three diversified groups of follicle cells,
77 and putative oogonial stem cells organized in germ cell cysts. Our cross-species
78 comparison revealed the presence of potentially conserved ovarian cell types, including
79 a granulosa-like population. Last, we report conserved signaling pathways involved in
80 oogenesis, as well as an intrinsic hypothalamic-like and gonadotropic-like signaling
81 system operating between oogonial stem cells and ovarian neurons which we propose
82 may be analogous, or possibly homologous, to the vertebrate HPG axis.
83

84 **Materials and Methods**

85 **Animal husbandry, ovary isolation, *in vitro* culture**

86 Adult *Patiria miniata* were obtained from South Coast Bio (San Diego, CA, USA) and
87 Monterey Abalone Company (Monterey, CA, USA). The animals were maintained in
88 temperature controlled (15°C) circulating seawater aquariums at the Marine Resources
89 Center (MBL, MA, USA). Ovarian fragments were surgically isolated through the oral side
90 of the sea star's arm using a Stoelting™ Sterile Disposable Scalpel, No.11 and ovaries
91 were collected using forceps in Eppendorf tubes containing filter sea water (FSW). For
92 the single cell RNA sequencing experiments the ovaries were used immediately. For the

93 rest of the experiments of the manuscript, ovaries were kept in FSW 10 µg/ml
94 trimethoprim and 50 µg/ml sulfamethoxazole at 15°C as previously described (12).
95
96 **Ovary dissociation**
97 Dissociation of isolated sea star intact ovarian lobes into single cells was performed as
98 previously described with minor modifications (13). Briefly, ovarian fragments were
99 transferred with forceps to a petri dish containing Ca^{2+} Mg^{2+}-free artificial sea water
100 (CaMg-free ASW) and allowed to settle for 3 minutes (min). Then the ovary was
101 transferred to an Eppendorf tube containing the dissociation buffer (1M glycine, 0.02M
102 EDTA, in CaMg-free ASW) and incubated for 10 min. Dissociation was promoted through
103 gentle pipette aspiration every 2 min. Once dissociation was complete, cells were spun
104 down with a swing bucket centrifuge at 500g for 10 min and washed twice with CaMg-
105 free ASW. Propidium Iodide and Fluorescein diacetate were used to assess cell viability
106 and only cell suspensions with cell viability ≥ 90 % were further processed. Single cells
107 were passed through a 40 µm cell strainer to remove aggregates. The number of cells
108 was estimated using a hemocytometer and diluted according to the manufacturer's
109 protocol (10X Genomics). During the entire process, specimens were kept on ice, except
110 for the centrifugations in which they were kept at 4°C. The isolated cells were loaded on
111 the 10x Genomics Chromium Controller according to the manufacturer's instructions and
112 cDNA libraries were generated using the Chromium Single Cell 3' Reagent Kit (v3.1
113 Chemistry Dual Index). Specimens were sequenced by the Azenta Life Sciences
114 (Burlington, MA) sequencing service using the Illumina NextSeq 550 with a maximum
115 read length 2 x 150 bp at a resolution of 350M PE reads.
116
117 **Single cell RNA sequencing mapping of reads and data analysis.**
118 Single cells from ovaries originating from three different animals were processed using
119 the 10X Genomics Chromium scRNA-seq capturing system. The libraries generated were
120 biased towards early oogenesis since the 10X Genomics Chromium capturing system
121 allows for the capture of cells up to 40 µm, which means that in our single cell atlas the
122 maximum oogonium size represented is 40 µm. Fully grown oocytes in *Patiria miniata* are
123 ~170 µm. *Patiria miniata* genome version 3.0 (14) was used for single cell RNA

124 sequencing read mapping. The corresponding annotation was modified to contain only
125 protein coding entries using AGAT v0.7.0 (15) and Linux command line tools GNU
126 coreutils v8.26. Cell Ranger Software Suite v7.1.0 (16) was used to create the index from
127 the genome FASTA file and the annotation GTF file as well as for mapping with --no-bam
128 and --nosecondary flags, with all other settings left as default so the number of cells was
129 estimated automatically by Cell Ranger. Cell Ranger output files were loaded in R Studio
130 and processed with the Seurat pipeline (17). Seurat objects were created by excluding
131 cells containing genes that are transcribed in less than three cells and cells that have less
132 than a minimum of 400 and a maximum of 5000 transcribed genes. Next the Seurat
133 objects were normalized, and variable genes were found through the variance stabilizing
134 transfer (VST) method with a maximum of 2000 variable features. The three different
135 objects were integrated through identification of gene anchors (FindIntegrationAnchors).
136 Following integration, scaling and principal component analysis (PCA) were performed.
137 Jackstraw was used to evaluate PCA significance. Uniform Manifold Approximate and
138 Projection (UMAP) was used to perform clustering dimensionality reduction. The final
139 object consisted of 35,877 cells. The FindAllMarkers command was used to identify
140 differentially expressed marker genes. The average expression of genes of interest were
141 visualized using the DotPlot and DoHeatmap commands included in the Seurat R
142 package. To compare the *Patiria miniata* ovary integrated single cell atlas with the publicly
143 available human (18), mouse (19), zebrafish (20), sea urchin (21) and fruit fly (22) ovarian
144 atlases as well as with the mouse pituitary gland atlas (23) and the sea urchin larva one
145 (13) SAMap v1.02 (24) was used as previously described (25). For the mouse, zebrafish,
146 fruit fly and sea urchin (ovary and larva) datasets the already available rds files were
147 used, while for the human fetal ovary and the mouse pituitary gland datasets clustering
148 analysis was performed similar to what was previously described (18,23). The average
149 score of genes of interest was performed using the AddModuleScore function
150 incorporated in the Seurat R package. The oogenesis trajectory was performed using the
151 R package Monocle3 (26). The package EnhancedVolcano was used to visualize the
152 differentially expressed genes between the germ cell cysts and oocytes along the
153 trajectory, while the R packages topGO and clusterProfiler were used for the GO
154 enrichment analysis.

155 **Light sheet microscopy/Segmentation 3D analysis**

156 Ovarian samples were mounted individually in Fluidflon FEP tubes (Proliquid 1.6x2.4mm)
157 using 1% low gelling agarose (Sigma-Aldrich A0701, type VII-A) with their elongated
158 morphology parallel to the tube. A Zeiss Lightsheet 7 was used to acquire multiple-view
159 data. It was equipped with a 10x/0.5 W Plan-Apochromat detection objective and two
160 10x/0.2 air illumination objectives producing two light-sheets 5.8 µm thick at the waist and
161 12µm thick at the edges of a 1100 µm x 1100 µm field of view. Illumination mode was
162 dual (mean fused) with active pivot scan. Samples were imaged from five views (72
163 degrees apart) and Zoom factor 0.8. Each z-stack has a pixel frame of 1920x1920 and a
164 voxel size of 0.57 µm x 0.57 µm x 1.8 µm. Each optical slice was acquired with a
165 combination of 405, 488, and 561 nm laser with following filter settings: 405nm: EF1 - BP
166 420-470, CAM BS - SBS LP 490; 488 nm: EF1 - BP 505-545, CAM BS - SBS LP 560,
167 561 nm: EF1 - BP 575-615, CAM BS - SBS LP 640. For registration of multi-view
168 acquisitions and fusion plus deconvolution of the registered data, the Fiji plugin
169 BigStitcher v2.3.4 (27) was used with standard settings. Image segmentation, 3D-
170 reconstructions and data analysis were performed using the Amira software package (FEI
171 Visualization Sciences Group Thermo Fisher Scientific), version 2024.1. Morphological
172 features such as muscles and nuclei were segmented semi-automatically using various
173 tools in Amira, such as "Thresholding" and "Magic Wand". Oocytes and germ cell cysts
174 were primarily segmented manually. Volumes of oocytes and germ cell cysts were
175 measured using the “Material Statistic” tool. Visualization of all segmented
176 reconstructions was achieved using tools like “Volren”, "Surface Rendering" and “Surface
177 View” within the software package.

178

179 **Immunohistochemistry (IHC) and fluorescent stainings**

180 Ovarian fragments were fixed with 4% PFA in FSW for 15-20 min at room temperature
181 (RT). Specimens were washed twice with FSW and five times with PBS supplemented
182 with 0.1 % Tween (1x PBST). Next, samples were incubated in blocking solution [1 mg/ml
183 Bovine Serum Albumin (BSA) and 4 % sheep serum (SS)] in PBST for one hour at RT.
184 Blocking solution was removed and primary antibodies were added in the appropriate
185 dilution in blocking solution and incubated overnight at 4°C. 1E11 (gift from Dr. Ina

186 Arnone) was used in a 1:20 dilution, anti-acetylated tubulin (Sigma) 1:100, anti-DM1α
187 (Developmental Studies Hybridoma bank) 1:100, anti-alpha tubulin (Sigma) 1:100, anti-
188 MHC (PRIMM) 1:50, anti-serotonin (Sigma) 1:500, anti-TH (Sigma) 1:100m and anti-
189 Myosin II (Developmental Studies Hybridoma bank) (1:50). Samples were washed five
190 times with 1x PBST (15 min each) and incubated for one hour at RT with secondary
191 antibodies (AlexaFluor) diluted 1:1000 in PBST. Samples were washed five times with 1x
192 PBST. In cases where phalloidin (Invitrogen) was used, it was diluted 1:20 (from a 40x
193 stock solution) in 1x PBST and allowed to incubate overnight at 4°C. For WGA staining
194 (Invitrogen) a working solution of 5 µg/mL was prepared, and the specimens were
195 incubated overnight at 4°C. Ovaries were washed five times with 1x PBST, nuclei were
196 stained with DAPI (1 µg/mL), and specimens were mounted for imaging. During the entire
197 procedure the interval of each wash was 15 min.
198
199 **Whole mount Hybridization Chain Reaction (HCR)**
200 HCR was performed according to previous protocols (28) with minor modifications.
201 Probes were designed either by Molecular Instruments or HCR 3.0 Probe Maker (29).
202 Ovarian fragments were fixed in 4% PFA in Fixative Buffer (0.1M MOPS, 0.5M NaCl,
203 2mM EGTA, 1mM $MgCl_2$ and 1x PBS) for 1 hour at room temperature (RT). Specimens
204 were washed three times with Fixative Buffer (without PFA) at RT. Samples were washed
205 twice with 100% methanol, transferred into fresh 100% methanol, and placed at -20°C for
206 long term storage. Specimens were rehydrated in 75%, 50%, 25% methanol in RNAase
207 free water on ice (each for 10 min). Next, ovaries were washed four times for 5 min each
208 in RNase free 1x PBST. Ovaries were treated with permeabilization buffer (1.0% SDS,
209 0.5% Tween, 50 mM Tris-HCl (pH 7.5), 1.0mM EDTA (pH 8.0), 150 mM NaCl) and
210 incubated for 1h at RT. Next, specimens were washed four times for 5 min each in 1x
211 PBST. Pre-heated (37°C) Probe Hybridization Buffer (PHB) was added to the samples
212 and incubated for 3 hours at 37°C. PHB was exchanged with PHB containing in total 0.04
213 µM of each probe and specimens were left to incubate for one day at 37°C. Following
214 hybridization, samples were washed 4 times with pre-heated Probe Wash Buffer (PWB)
215 for 5 min each, followed by two washes with PWB for 30 min each at 37°C. Samples were
216 then washed two times with 5x SSCT (5x Saline Sodium Citrate and 0.1% Tween) and

217 two times with 1x SSCT (1x Saline Sodium Citrate and 0.1% Tween) each for 5 min. Next,
218 specimens were incubated with Amplification Buffer for 30 min at RT, hairpins were added
219 to the specimens according to manufacturer's guidelines and incubated overnight at RT
220 in the dark. Lastly, samples were washed twice with 1x SSCT for 5 min, two more times
221 for 30 min and four times with 1x PBST. Nuclei were stained with DAPI (1 µg/mL), and
222 specimens were mounted for imaging.
223
224 **Fluorescent *in situ* hybridization (FISH)**
225 FISH and antisense RNA probes design was performed as previously described (30,31).
226 In brief, ovaries were fixed in 4% PFA in MOPS Buffer for 1 hour at RT. Samples were
227 washed five times with MOPS buffer, gradually dehydrated (20%, 50% ethanol) and
228 stored in 70% ethanol and kept at -20°C for long term storage. Specimens were gradually
229 rehydrated (50%, 20% ethanol) and washed five times with MOPS Buffer. At this step
230 ovaries were dissected to smaller pieces using micro scissors. Specimens were then pre-
231 hybridized for 3 hours at 65°C, followed by a 48 hour period of probe hybridization. Next,
232 specimens were washed five times with MOPS Buffer and incubated in blocking solution
233 (Akoya Biosciences) for 30 min at RT. Next, specimens were transferred to a solution
234 containing the anti-Digoxigenin (Roche) antibody diluted 1:1000 in blocking solution. The
235 antibody solution was removed, samples were washed with MOPS Buffer five times and
236 the signal was developed using fluorophore conjugated tyramide technology (TOCRIS).
237 Nuclei were stained with DAPI (1 µg/mL), and specimens were mounted for imaging.
238
239 **EdU labeling**
240 Click-It EdU Cell Proliferation Kit for Imaging Alexa Fluor 488 (Thermo Fisher Scientific)
241 was used and was combined with either HCR or IHC as previously described (13,32).
242 Isolated intact ovarian fragments were treated with EdU at a final concentration of 20 µM
243 in FSW with 10 µg/ml trimethoprim and 50 µg/ml sulfamethoxazole and allowed to
244 incubate for 2 days at 15°C. Depending on whether the EdU cell proliferation was
245 combined with HCR or IHC specimens were fixed accordingly as described in their
246 respective sections above. To develop the EdU signal, the Click-iT reaction mix was
247 prepared according to the manufacturer's guidelines. In cases where the EdU assay was

248 combined with HCR after the washes with PWB, specimens were washed twice with 3%
249 BSA in PBST for 15 min at RT. Next the Click-iT reaction mix was added and incubated
250 for 30 min in the dark at RT. After this step the HCR procedure was carried out as
251 described above. For combination of the EdU Cell Proliferation assay with
252 immunostaining the ovaries were fixed in 4 % PFA in FSW for 15 min at RT and washed
253 five times with PBST. PBST was removed and the reaction mix was added to the samples
254 for 30 min (RT). Specimens were washed five times with PBST, mounted for imaging.
255

256 **Results**

257 **The structural organization of the *Patiria miniata* adult ovary**

258 We first sought to define the structure of its ovary, which is multi-lobed and optically
259 translucent (**Fig. 1B**). We stained for F-actin with phalloidin as a cell boundary marker
260 and acetylated tubulin to visualize cilia (**Fig. 1C**). Each ovarian lobe is a hollow tube that
261 consists of a thin, tightly packed epithelial cell layer with long motile cilia (**Fig. 1B**). We
262 also identified cells organized in plexus-like structures resembling a nerve net underneath
263 the epithelial layer that are positive for synaptotagmin 1, a pan-neuronal marker in
264 echinoderms (**Fig. 1D, S1A, E-H**). We also identified ovarian neurons in the related sea
265 urchin *Strongylocentrotus purpuratus* (**Fig. S1I-J**) and the sea cucumber *Holothuria*
266 *tubulosa* (**Fig. S1K-L**), arguing that these are a conserved cell type across echinoderms.
267 We also identified extensive musculature below and in close proximity to the nerve net
268 (**Fig. 1E, S1B**), which is likely responsible for the contraction of the ovary during spawning
269 (33). We observed axonal projections in close proximity to the muscle layer, which may
270 regulate their contraction (**Fig. S1E-F, I-J**). Below the muscle layer and within the lumen,
271 we detected oocytes at different stages of maturation enwrapped by follicle cells, which
272 are filamentous in nature and ciliated (**Fig. 1F, Fig. S1C-D**).
273

274 We determined the stages of oocyte development, and the nature of oocyte-follicle
275 complexes. Early small oogonia are spatially organized in closely associated groups with
276 an average size of 8-16 μm (**Fig. 1G, Fig. S2A-B**). These groups were found in all ovaries
277 tested, although their number varied with different individuals. The chromatin morphology
278 of these cells was distinct, with condensed DNA concentrated towards the nuclear

279 periphery. This may be consistent with the leptotene to zygotene stage of meiosis, in
280 which chromosomes adopt a bouquet configuration (34). The cells within these groups
281 were compact with intense actin staining at the cell boundaries, and surrounded by small
282 somatic nuclei that do not intercalate within the cluster (**Fig. 1G**). This organization
283 resembles germ cell nests or cysts that are found in other species, including fruit flies and
284 mammalian fetal ovaries (35). Similar structures were observed by electron microscopy
285 in the ovaries of the phylogenetically distant sea star *Asterias rubens* (36). Co-staining
286 for F-actin and membrane lectins revealed cortical channel-like structures between
287 distinct oogonia within the germ cell groups (**Fig. 1H-J**). Such an organization strongly
288 resembles the intercellular bridges that physiologically connect the germ cells within the
289 germ cell cysts in mammals and protostomes, allowing for the exchange of the germ
290 plasm and suggests that germ cells are organized in cysts also in a non-chordate
291 deuterostome. Therefore, from here on we refer to these groups as "cysts".
292
293 To test the germline nature of these cysts, we performed HCR for the conserved germ
294 cell factor *nanos1,* and the yolk protein *vtg2*, which is expressed in sea star follicle cells
295 in other echinoderms (37–39). We found that *nanos1* is expressed specifically in oocytes
296 of all sizes as well as in the cysts (**Fig. 1K**). *vtg2* was expressed by the follicle cells that
297 surround the oocytes. We also found that the *vtg2*+ follicle cells enwrap the cysts as a
298 whole, while none of the cells within the cysts are individually enwrapped (**Fig. 1K**). This
299 configuration further resembles the germ cell cysts observed in vertebrates, suggesting
300 that sea star adult oogenesis may share conserved features. Co-staining for *nanos1* and
301 *vtg2* also enabled us to ask what is the smallest oocyte size necessary to form a primary
302 follicle. We found that the smallest *nanos1*+ oocytes are located next to germ cell cysts
303 and by using the diameter of these oocytes as a proxy to calculate the size and volume
304 we found they are within the range of 17-42 µm (**Fig. S2C-D**).
305
306 We next asked how oogenesis is spatially organized within the ovarian lobe. Is there a
307 defined stem cell niche, or is oogenesis instead uniformly distributed? To test this, we
308 used large volume light sheet microscopy on entire ovarian lobes (**Fig. 1L-M, Fig. S2G**).
309 Segmentation and 3D reconstruction revealed that oogenesis is spatially polarized from

310 outside to inside. Germ cell cysts and smaller oocytes were localized entirely to the
311 periphery of the lobe interior, but were broadly distributed. Fully grown oocytes in
312 prophase I arrest, instead, were centrally located within the lumen (**Fig. 1L-M, Fig. S2G**).
313 Quantification of segmented cell volumes found that the diameter of the entire germ cell
314 cysts ranges from 27-56 µm, of the small oocytes from 17-106 µm and of the pre-GVBD
315 ones from 107-187 µm (**Fig. S2E-F**). Altogether, these results define the cell type
316 organization of the sea star ovary at a molecular level and the oocyte size distribution
317 during oogenesis (**Fig. 1N, Fig. S2A-F)**. Moreover, our data provide molecular evidence
318 for the presence of germ cell cysts and show how *P. miniata* oogenesis is spatially
319 oriented within the ovary.

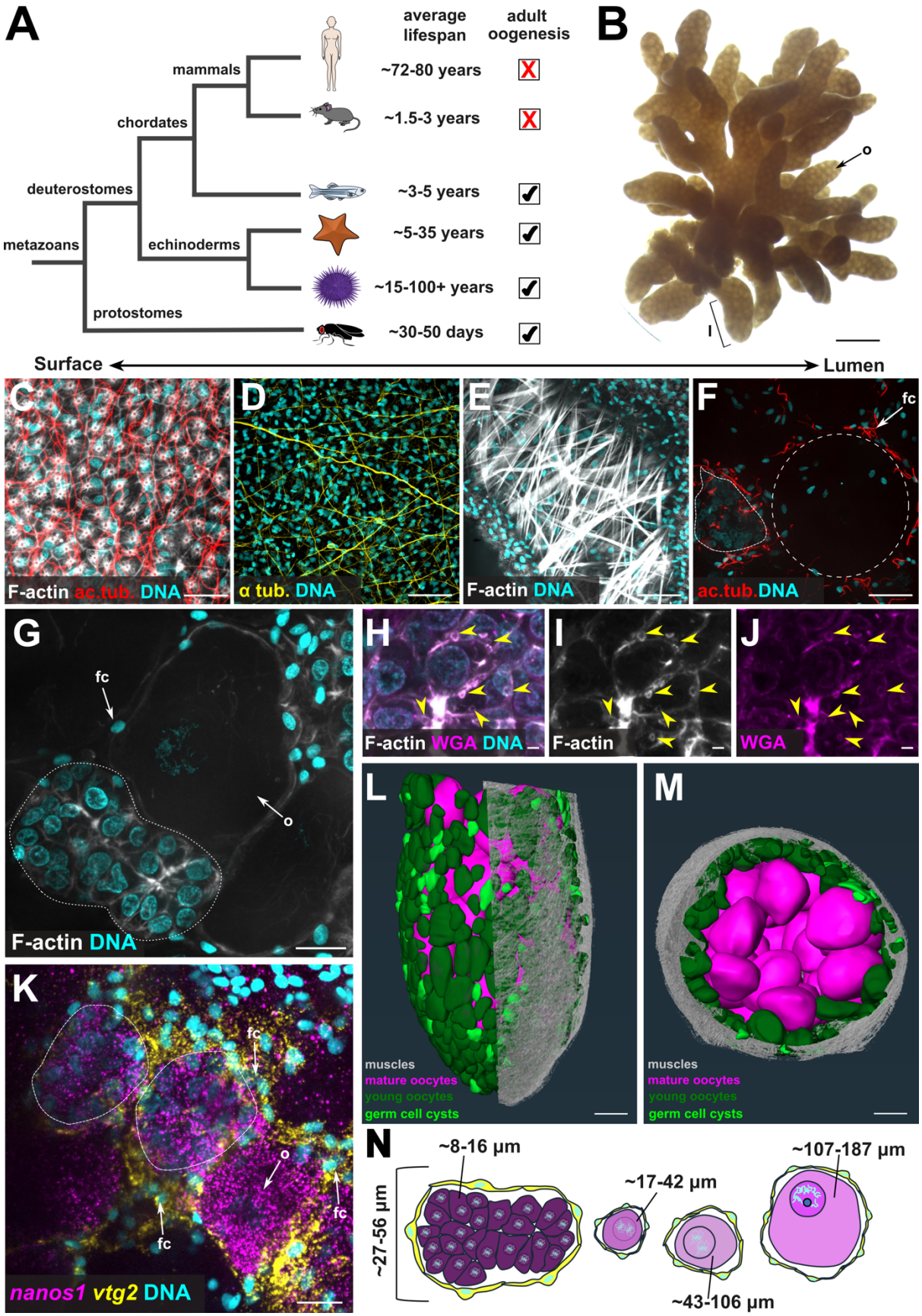
A
average lifespan
adult oogenesis
mammals
chordates
deuterostomes
metazoans
echinoderms
protostomes
~72-80 years
~1.5-3 years
~3-5 years
~5-35 years
~15-100+ years
~30-50 days
B
o
l
Surface
Lumen
C
F-actin ac.tub. DNA
D
α tub. DNA
E
F-actin DNA
F
fc
ac.tub.DNA
G
fc
o
F-actin DNA
H
F-actin WGA DNA
I
F-actin
J
WGA
K
fc
o
fc
fc
nanos1 vtg2 DNA
L
muscles
mature oocytes
young oocytes
germ cell cysts
M
muscles
mature oocytes
young oocytes
germ cell cysts
N
~8-16 µm
~27-56 µm
~17-42 µm
~43-106 µm
~107-187 µm

320

321 **Figure 1. Molecular characterization of the *P. miniata* ovary.** (**A**) Phylogenetic tree showing the
322 evolutionary relationships of *P. miniata* with other metazoan experimental systems. (**B**) *P. miniata* ovarian
323 explant. Scale bar is 1 mm. (**C**) Phalloidin and acetylated tubulin staining to label cell boundaries and cilia.
324 Scale bar is 20 µm. (**D**) IHC for α-tubulin labeling the ovarian nerve plexus. Scale bar is 40 µm. (**E**) Phalloidin
325 staining showing ovarian muscle fibers. Scale bar is 40 µm.(**F**) Acetylated tubulin labeling cilia on the follicle
326 cells. Dotted circle indicates oocytes, while germ cell cysts are outlined with dotted lines. Scale bar is 20
327 µm. (**G**) Phalloidin staining labeling the cell boundaries of the germ cell cysts. Germ cell cysts are outlined
328 with dotted lines. Scale bar is 20 µm. (**H-J**) Phalloidin and WGA lectin co-staining labeling the cell
329 boundaries and membranes. Yellow arrowheads indicate intercellular bridge-like structures. Scale bar is 1
330 µm. (**K**) HCR for *nanos1* (magenta) and *vtg2* (yellow) labeling the entire germ lineage and follicle cells
331 respectively. Germ cell cysts are outlined with dotted lines. Scale bar is 20 µm. Nuclei were labelled with
332 DAPI (cyan). (**L-M**) 3D rendering of segmented germ cell cysts and oocytes. Scale bar is 100 µm. Ovary
333 seen from the lateral (I) and top (J) views. (**N**) Schematic summary of the germ cell cyst, young oocyte and
334 mature oocyte size distributions in the *P. miniata* ovary. fc, follicle cells; l, lobe; o, oocytes.
335

336 **The *P. miniata* ovary consists of nine molecularly distinct cell type groups**

337 Having defined the overall structures of the ovary, we next sought to determine the
338 molecular identities of its constituent cell types with scRNA-seq (**Fig. 2A, Fig. S3A**). We
339 used ovaries from three independent *Patiria miniata* females (**Fig. S3B-C**). One ovary
340 originated from an individual in which spawning was induced 2 months prior to ovarian
341 isolation, one was highly enriched in germ cell cysts and early oocytes, and one consisted
342 mostly of fully grown oocytes. For each ovary used, the size distribution of their
343 oogonia/oocytes was determined by dissociating the ovaries and manually measuring the
344 oogonia/oocytes diameter to estimate their volume (**Fig. S3B-C**). Computational analysis
345 and integration of the sequenced libraries yielded an atlas of 35,877 cells distributed in
346 twenty-seven clusters or cell states (**Fig. 2A, Fig. S3A**).
347

348 We next inferred the cell type identities of the twenty-seven clusters using the average
349 expression of differentially expressed marker genes**,** and gene homologs known to label
350 ovarian cell types, in echinoderms and other organisms. (**Fig. 2B)** We curated 9 cell type
351 groups expressing genes corresponding to endothelial and ciliated cells (*btub2/3, cfap77,*
352 *dhc2, col1a, vwf*) (13,40,41), mammalian granulosa cells (*tgfb2, foxl2, inhbb, cyp26, foxo,*
353 *gata4*) (1,42–45), echinoderm follicle cells (*vtg2, vtg5*) (39), mammalian theca cells
354 (*mmp14, angpt1, star, cyp17a1, vegfa, fgf18*) (46–50), muscles (*mhc, mlck, tnn1*) (13),

355 immunocytes (*lyz, mpeg1, bpi, cd151*) (51–54), neurons (*syt1, smp, pplnp, oxy/vp, hdc*)
356 (13,55,56) and germ cells/oocytes (*nanos1, nanos3, boll, piwi1, msl3, sycp1, figla, ddx4,*
357 *sox2, pum2*) (37,38,57–64). We found that most cell states were equally distributed
358 amongst the three ovary samples (**Fig. S3D**) with the exception of clusters 5, 9, 10, 11,
359 12 and cluster 4, identified as follicle cells and epithelium, respectively, which
360 predominantly originated from the previously spawned ovaries of female 1. Germ cell cyst
361 clusters 13 and 14 were also enriched in sample 2, which was used for the 3D volume
362 analysis (**Fig. 1I-K**) and contained numerous germ cell cysts. Therefore, our single cell
363 atlas reflects the experimentally validated reproductive states of the ovaries used. With
364 this confidence in our dataset, we next sought to spatially map their location within intact
365 ovaries using HCR and FISH (**Fig. 2C-H. Fig. S3E-I**).
366
367 We first examined genes expressed in follicle cells, which enwrap and support oocytes
368 as they develop. Using HCR, we detected *vtg2* (a previously validated marker) and the
369 signaling molecule *tgfb2* in follicle cells, with the mammalian theca marker *tgfb2* (65)
370 being expressed in a subset of them (**Fig. 2C-D**). We also detected *foxl2*, a known
371 mammalian granulosa cell transcription factor, in follicle cells (**Fig. 2E**). Therefore, the
372 clusters that contain *foxl2* (clusters 5-8, 23-24), *tgfb2* (clusters 5, 7-8, 22, 24-25) and *vtg2*
373 (clusters 5-8, 9-12, 23) transcripts were confirmed to correspond to the partially non
374 overlapping follicle cell groups as identified by scRNA-seq.
375
376 We next turned to the putative germ line clusters. The transcription factor *figla*, which
377 functions in mammalian oogenesis, was detected exclusively in the germ cell lineage
378 including cysts and oocytes (**Fig. 2F**). Similar results were obtained for the germline
379 factors *piwi1* and *nanos3* (**Fig. 2G, Fig. S3D-D'**). Surprisingly, we did not detect the
380 conserved germ line RNA helicase *ddx4/vasa* in the germ cell cysts, though it was
381 detected in all other oocyte stages (**Fig. 2H**). This result suggests that *ddx4/vasa*
382 transcription is activated only once the primary follicle is formed. These expression
383 patterns are consistent with the single-cell predictions and suggest the presence of two
384 cell groups: the germ cell cysts (clusters 13 and 14) and early oocytes (clusters 15, 16,
385 17, 18 and 19). To further validate our clustering analysis, we examined *syt1* expression,

386 which was unexpectedly predicted to be present not only in the nervous system but also
387 in germ cell cysts and oocytes. HCR confirmed *syt1* in the nerve net as well as in the
388 germ cell cysts and oocytes (**Fig. S3F-G'**), while a positive control in *P. miniata* larvae
389 and post-metamorphic juveniles verified the probe specificity, showing *syt1* expression in
390 the nervous system as reported in other echinoderms (**Fig. S3H, I**). Taken together, our
391 spatial and transcriptomic analyses enabled us to identify and map nine cell type groups
392 distributed in twenty-seven clusters (**Fig. 2I**).

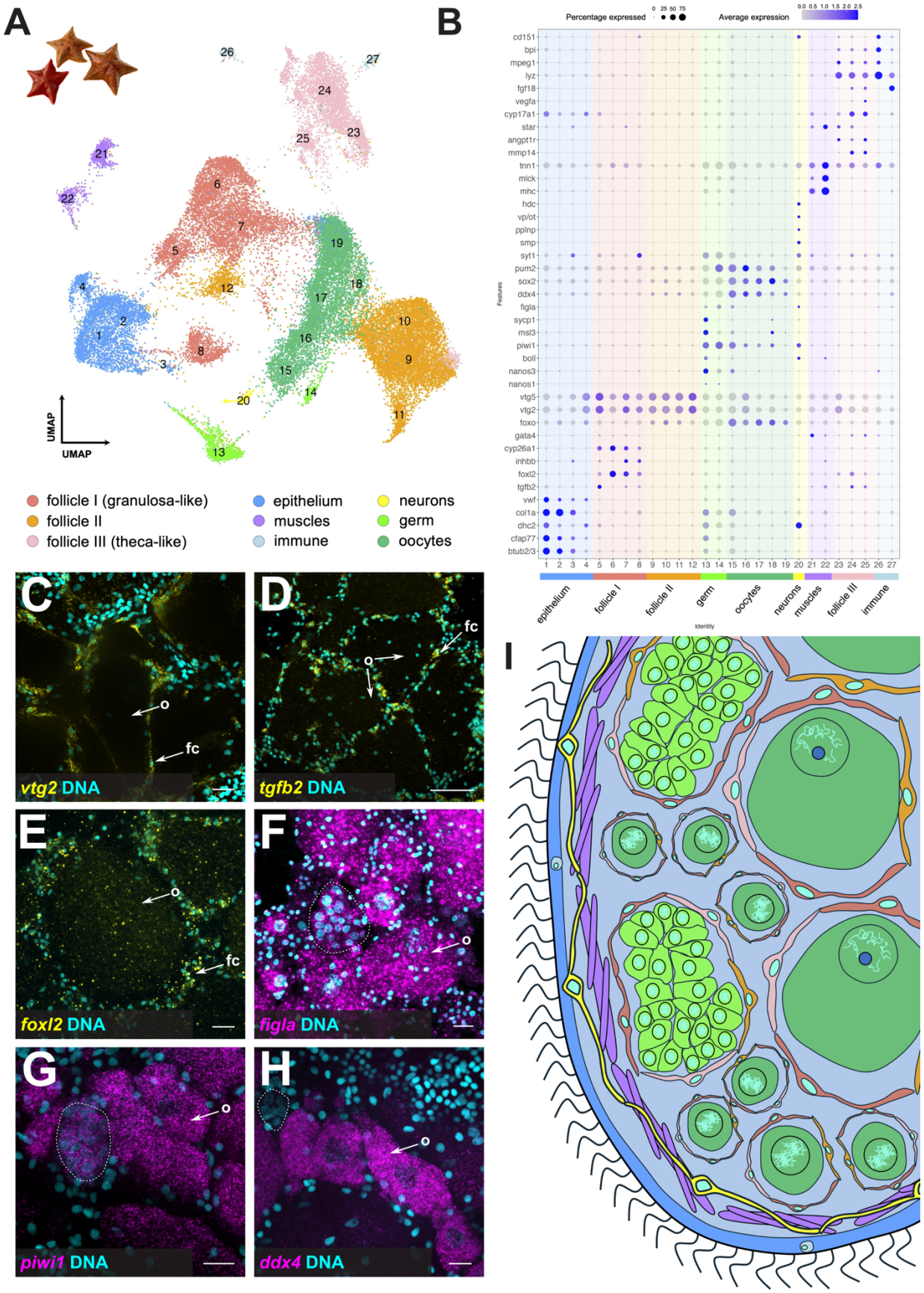
A
B
UMAP
UMAP
follicle I (granulosa-like)
follicle II
follicle III (theca-like)
epithelium
muscles
immune
neurons
germ
oocytes
Percentage expressed
Average expression
Features
Identity
epithelium
follicle I
follicle II
germ
oocytes
neurons
muscles
follicle III
immune
C
vtg2 DNA
D
tgfb2 DNA
E
foxl2 DNA
F
figla DNA
G
piwi1 DNA
H
ddx4 DNA
I

393

394 **Figure 2. Cell type/state diversity of the *P. miniata* adult ovary. (A)** Integrated UMAP of the three
395 different scRNA-seq libraries. Color code is indicative of different cell type groups. **(B)** Dotplot showing the
396 average expression of known echinoderm cell type markers as well as genes labeling ovarian and
397 associated cell types in other organisms. Color code is the same as in panel A. **(C-D)** HCRs for the follicle
398 cells markers *vtg2* (C) and *tgfb2* (D). **(E-F)** FISH using antisense probes for the transcription factors *foxl2*
399 *(E)* and *figla* (F) labelling the follicle cells and germ lineage respectively. Dotted circle in panel E is indicative
400 of oocytes, while germ cell cysts in panel F are outlined with dotted lines. Scale bars for panels C and E
401 are 20 µm, and for panel D 60 µm. **(G-H)** HCRs for the germ line markers *piwi1* and *ddx4*. Germ cell cysts
402 in panels G and H are outlined with dotted lines. Scale bars are 20 µm. **(I)** Schematic representation of the
403 ovary depicting the cell type groups revealed by our single cell RNA sequencing atlas. Color code is the
404 same as in panel A. fc, follicle cells; o, oocytes.
405

406 **Shared cell type toolkits between *P. miniata* and other deuterostomes**

407 How similar are sea star ovarian cell types to those of animals that diverged millions of
408 years ago? Our gene candidate-based analysis identified similarities—for instance, sea
409 star follicle cells (clusters follicle I and follicle III) express gene orthologs also found in
410 mammalian granulosa (*foxl2, inhbb, tgfb2, gata4*) and theca (*tgfb2, mmp14, angpt1r, star,*
411 *cyp17a1, vegfa, fgf18*) cells. To more broadly test this similarity, we used SAMap to
412 compare our atlas with published datasets of adult fruit fly, sea urchin, zebrafish, mouse,
413 and fetal human ovaries (**Fig. 3, S4**). As expected, sea star cluster 22 (muscle-related)
414 aligned with muscle clusters in all animal ovaries tested. This similarity is not unique to
415 ovarian muscles, as alignment with a sea urchin larval scRNA-seq dataset also revealed
416 strong similarity with esophageal muscles (**Fig. 3, S4**). We also identified similarity
417 between the sea star follicle cell I (cluster 6) and their follicular counterparts in fruit fly and
418 sea urchin (**Fig. 3A, S4A**). Surprisingly, despite substantial evolutionary distance, this
419 follicle cell cluster also aligned with follicle cells in zebrafish, and granulosa cells in both
420 mouse and human, although in the latter with lower alignment scores (**Fig. 3B,C, S4B**).
421 In addition, the sea star oocyte cluster 19 aligns with germ and oogonial cell clusters in
422 fruit fly, sea urchin, zebrafish and human (**Fig. 3A-C, S4A**). Zebrafish and mouse theca
423 cells aligned with sea star epithelial clusters, while zebrafish vasculature aligned to one
424 sea star follicle cluster (**Fig. 3B**). Similarities become scarcer when we compare the
425 ovaries of sea star with the adult mouse, which does not contain oogonial stem cells (66)
426 (**Fig. S4B**). However, when we compared the sea star ovary with the human embryonic

427 ovary, in which oogenesis is still occurring, we found that one human germ cell cluster
428 aligned with the sea star oocytes cluster 17 (**Fig. 3C**). We also detected similarities
429 between sea star follicle cells (I) with human endothelium, sea star follicle cells (III) with
430 human granulosa cells, as well as sea star epithelium with human stromal and theca cells
431 (**Fig. 3C**). A summary of the main findings can be found in (**Fig. 3D**). In support of the
432 specificity of the similarities we detected, comparison to the sea urchin larva, which
433 serves as a null comparison, yielded no strong hits apart from muscle (**Fig. S4C**). Overall,
434 our analysis has shown the existence of transcriptionally similar ovarian cell type
435 programs across phylogenetically distant organisms, suggesting the possible pre-
436 chordate origins of ovarian cell types, including follicle cells.

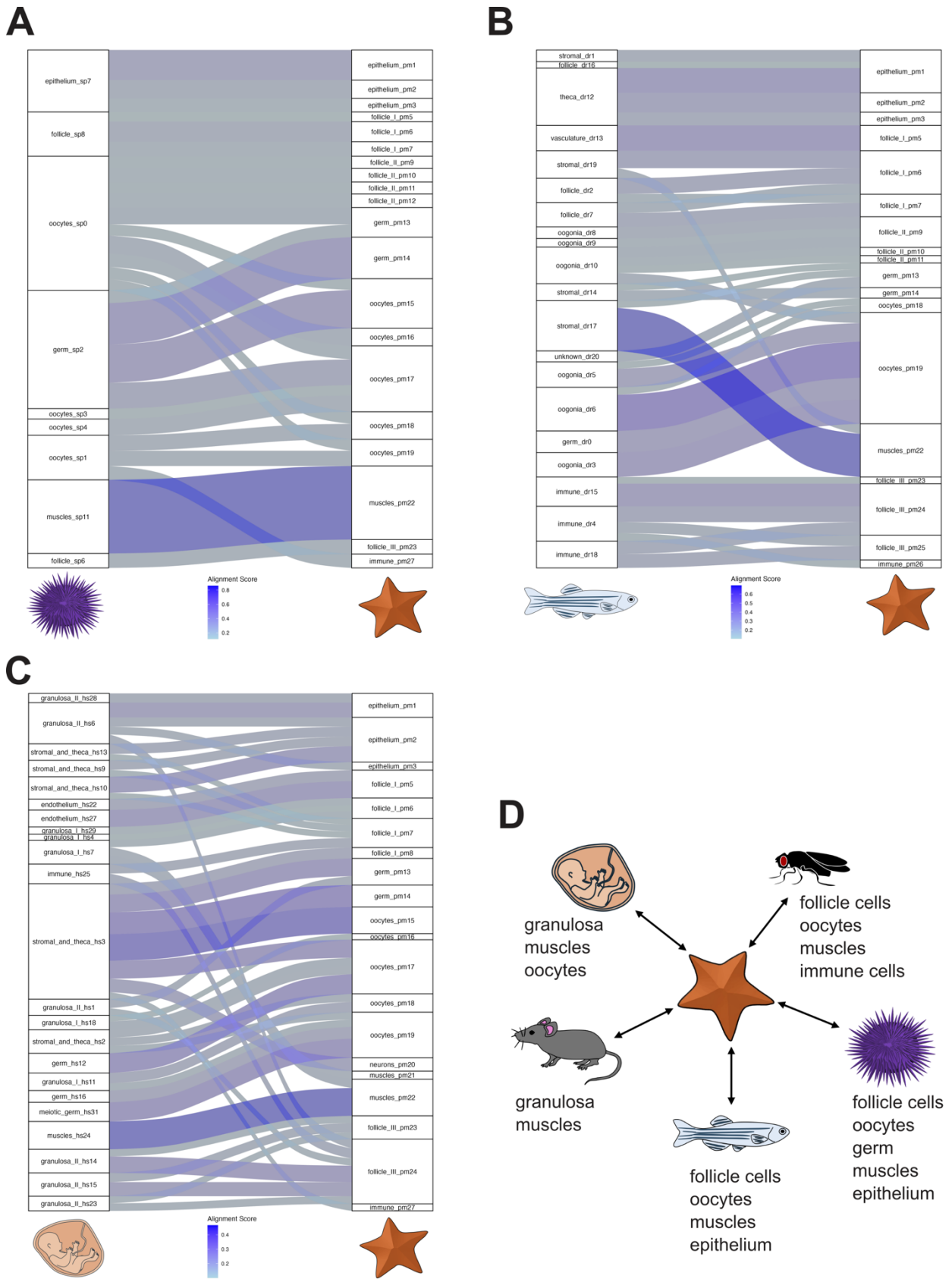
A
epithelium_sp7
follicle_sp8
oocytes_sp0
germ_sp2
oocytes_sp3
oocytes_sp4
oocytes_sp1
muscles_sp11
follicle_sp6
epithelium_pm1
epithelium_pm2
epithelium_pm3
follicle_I_pm5
follicle_I_pm6
follicle_I_pm7
follicle_II_pm9
follicle_II_pm10
follicle_II_pm11
follicle_II_pm12
germ_pm13
germ_pm14
oocytes_pm15
oocytes_pm16
oocytes_pm17
oocytes_pm18
oocytes_pm19
muscles_pm22
follicle_III_pm23
immune_pm27
Alignment Score
0.8
0.6
0.4
0.2
B
stromal_dr1
follicle_dr16
theca_dr12
vasculature_dr13
stromal_dr19
follicle_dr2
follicle_dr7
oogonia_dr8
oogonia_dr9
oogonia_dr10
stromal_dr14
stromal_dr17
unknown_dr20
oogonia_dr5
oogonia_dr6
germ_dr0
oogonia_dr3
immune_dr15
immune_dr4
immune_dr18
epithelium_pm1
epithelium_pm2
epithelium_pm3
follicle_I_pm5
follicle_I_pm6
follicle_I_pm7
follicle_II_pm9
follicle_II_pm10
follicle_II_pm11
germ_pm13
germ_pm14
oocytes_pm18
oocytes_pm19
muscles_pm22
follicle_III_pm23
follicle_III_pm24
follicle_III_pm25
immune_pm26
Alignment Score
0.6
0.5
0.4
0.3
0.2
C
granulosa_II_hs28
granulosa_II_hs6
stromal_and_theca_hs13
stromal_and_theca_hs9
stromal_and_theca_hs10
endothelium_hs22
endothelium_hs27
granulosa_I_hs29
granulosa_I_hs4
granulosa_I_hs7
immune_hs25
stromal_and_theca_hs3
granulosa_II_hs1
granulosa_I_hs18
stromal_and_theca_hs2
germ_hs12
granulosa_I_hs11
germ_hs16
meiotic_germ_hs31
muscles_hs24
granulosa_II_hs14
granulosa_II_hs15
granulosa_II_hs23
epithelium_pm1
epithelium_pm2
epithelium_pm3
follicle_I_pm5
follicle_I_pm6
follicle_I_pm7
follicle_I_pm8
germ_pm13
germ_pm14
oocytes_pm15
oocytes_pm16
oocytes_pm17
oocytes_pm18
oocytes_pm19
neurons_pm20
muscles_pm21
muscles_pm22
follicle_III_pm23
follicle_III_pm24
immune_pm27
Alignment Score
0.4
0.3
0.2
D
granulosa
muscles
oocytes
follicle cells
oocytes
muscles
immune cells
granulosa
muscles
follicle cells
oocytes
muscles
epithelium
follicle cells
oocytes
germ
muscles
epithelium

437

438 **Figure 3. Cross-species comparison of ovarian single cell atlases with SAMap.** Sankey plot depicting
439 the alignment scores between the adult sea star ovarian cell clusters with the adult sea urchin **(A)**, adult
440 zebrafish **(B)** and fetal human ovarian clusters **(C)**. **(D)** Summary of the cell types shared between sea star
441 and the taxa used for comparison. Alignment score is defined as the average number of mutual nearest
442 cross-species neighbors of each cell relative to the maximum possible number of neighbors. Alignment
443 scores equal or greater to 0.1 were considered significant.
444

445 **Identification and characterization of mitotic oogonial stem cells**

446 Having defined similar ovarian elements across species, we then asked what unique
447 features of the sea star ovary support its extreme reproductive capability, such as adult
448 oogonial stem cells (OSCs). To identify potential OSC populations, we computationally
449 scored for the co-expression of cell cycle-associated and meiotic genes with germline
450 marker genes (**Fig. 4A, S5A**). We found that the epidermal cell clusters 2 and 3, the germ
451 cell cysts clusters 13-14 and oocytes (15-19) express genes associated with G1/S phase
452 (including *cyclinD2, cyclinE, cdt1* and *pcna*), while the epidermal cluster 4, the follicle cell
453 clusters 9-12, the germ cell cyst cluster 14 and oocytes (15-19) express genes operating
454 during G2/M phase (including *cyclinA, cyclinB* and *bub3*) (**Fig. 4A**). Genes specific to
455 meiosis, such as *spo11, mlh1, hormad, sycp1, sycp2* and *sycp3* were expressed in the
456 germ cell cyst clusters 13-14 and oocyte clusters 15-19 (**Fig. 4A**). HCR for one of those
457 genes, *mlh1,* confirmed the predicted expression in both the germ cell cysts and the
458 oocytes (**Fig. 5SB**).
459

460 To directly test cell proliferation, we cultured ovarian lobes *in vitro* and performed EdU
461 cell proliferation assays (**Fig. 5SC-E**). We found cells undergoing DNA replication in both
462 somatic and germ cell populations. This included the ovarian epithelium, follicle cells, and
463 within germ cell cysts (**Fig. 5SC-E**). To further define the germ line population, we paired
464 EdU incorporation with HCR for *nanos1, piwi1* and *ddx4/vasa* (**Fig. 4B-E**). The EdU signal
465 was exclusively detected in *nanos1* and *piwi1* positive germ cell cyst nuclei, but not in the
466 *ddx4* positive growing oocytes. Altogether, these data revealed the presence of
467 replicating cells within the sea star ovary (**Fig. 4F**) and support our hypothesis of a self-
468 renewing oogonial stem cell pool in adult sea star ovaries.

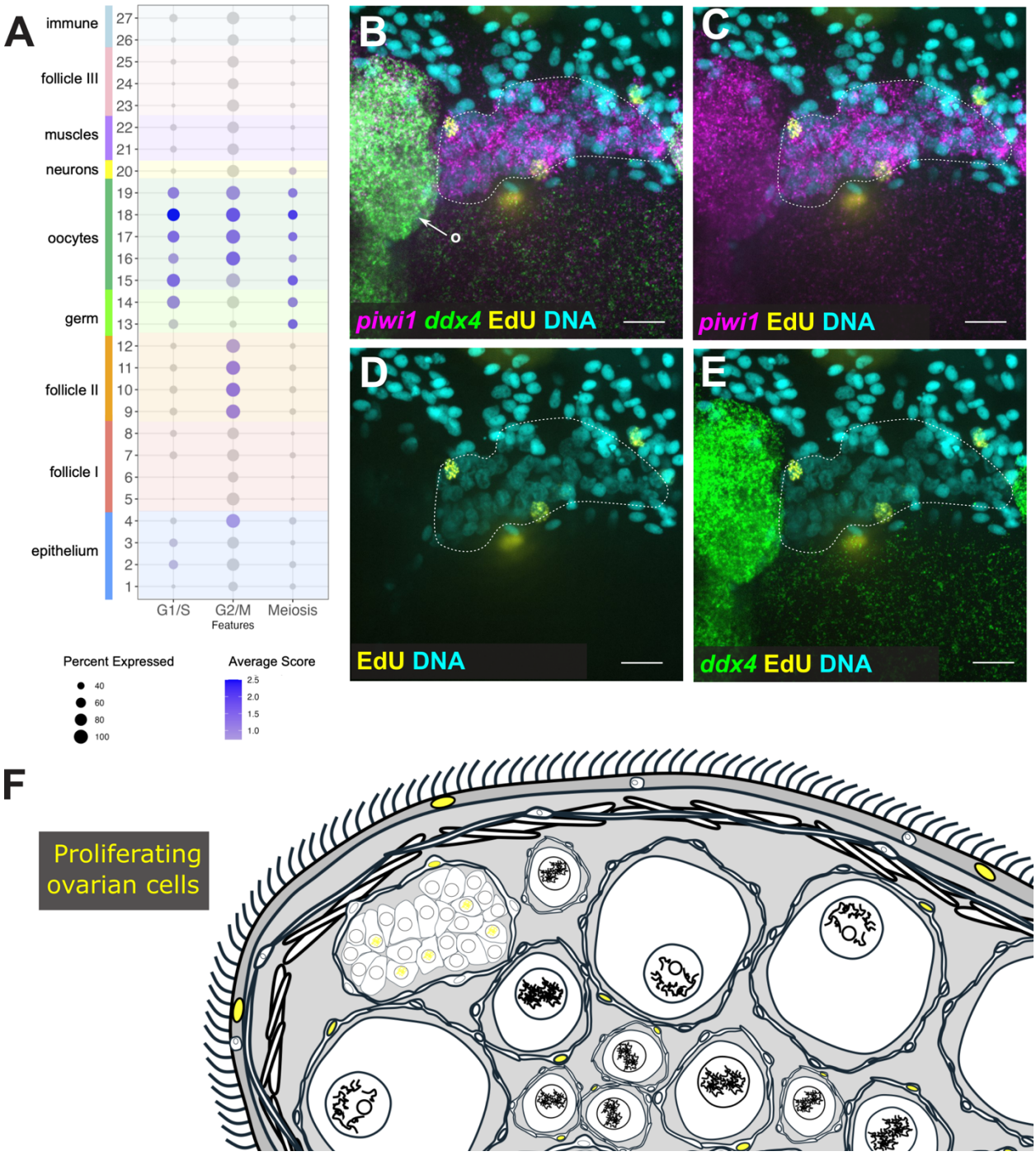

Figure 4. Identification of self-renewing oogonial stem cells. (A) Dotplot showing the average score of genes involved in G1/S, G2/M phases of the cell cycle and meiosis across the *P. miniata* ovarian cell type groups. (**B-E**) HCR for the germline markers *piwi1* and *ddx4* paired with the EdU proliferation assay. Scale bars are 20 µm. Nuclei were labelled with DAPI (cyan). Dotted lines outline the germ cell cyst in panels B-D. **(F)** Summary of the ovarian cell types undergoing mitosis as revealed by the EdU nuclear incorporation. o, oocytes.

476 We next asked how gene expression changes as oocytes develop. We used Monocle3
477 to identify a developmental trajectory linking the 7 germ line cell clusters (13, 14, 15, 16,
478 17, 18), from OSC to oocyte. Cluster 13 was chosen as the root because its molecular
479 signature and cellular morphology was most similar to typical germ cells, and because it
480 did not express *ddx4*, as experimentally validated by HCR (**Fig. 5C-E**). We found a
481 substantial number of genes that are upregulated in germ cell cysts and downregulated
482 in oocytes, and fewer that are more highly expressed in oocytes. (3378 genes
483 upregulated in cysts, 849 upregulated in small oocytes; **Fig. S6A**). Gene ontology (GO)
484 enrichment analysis shows that most of the cyst genes correspond to transcription and
485 translation factors, while many of the oocyte genes are related to splicing, protein
486 synthesis and transport. (**Fig. S6B-B', S7**). Among the genes also upregulated in the
487 germ cell cyst clusters are the transcriptional and epigenetic regulators *atrx1* and *cxxc1*.
488 Both genes are important for mammalian sexual differentiation and oogenesis
489 respectively (67–69). Plotting their average expression on the trajectory as well as HCR
490 for both genes confirmed their co-expression in the oocyte lineage and presence within
491 the germ cell cysts (**Fig. 5F-K, Fig. S6C-C'''**). Taken together our data highlight, for the
492 first time in echinoderms, distinct transcriptional differences occurring during the transition
493 from oogonia to early oocytes (**Fig. 5L**).

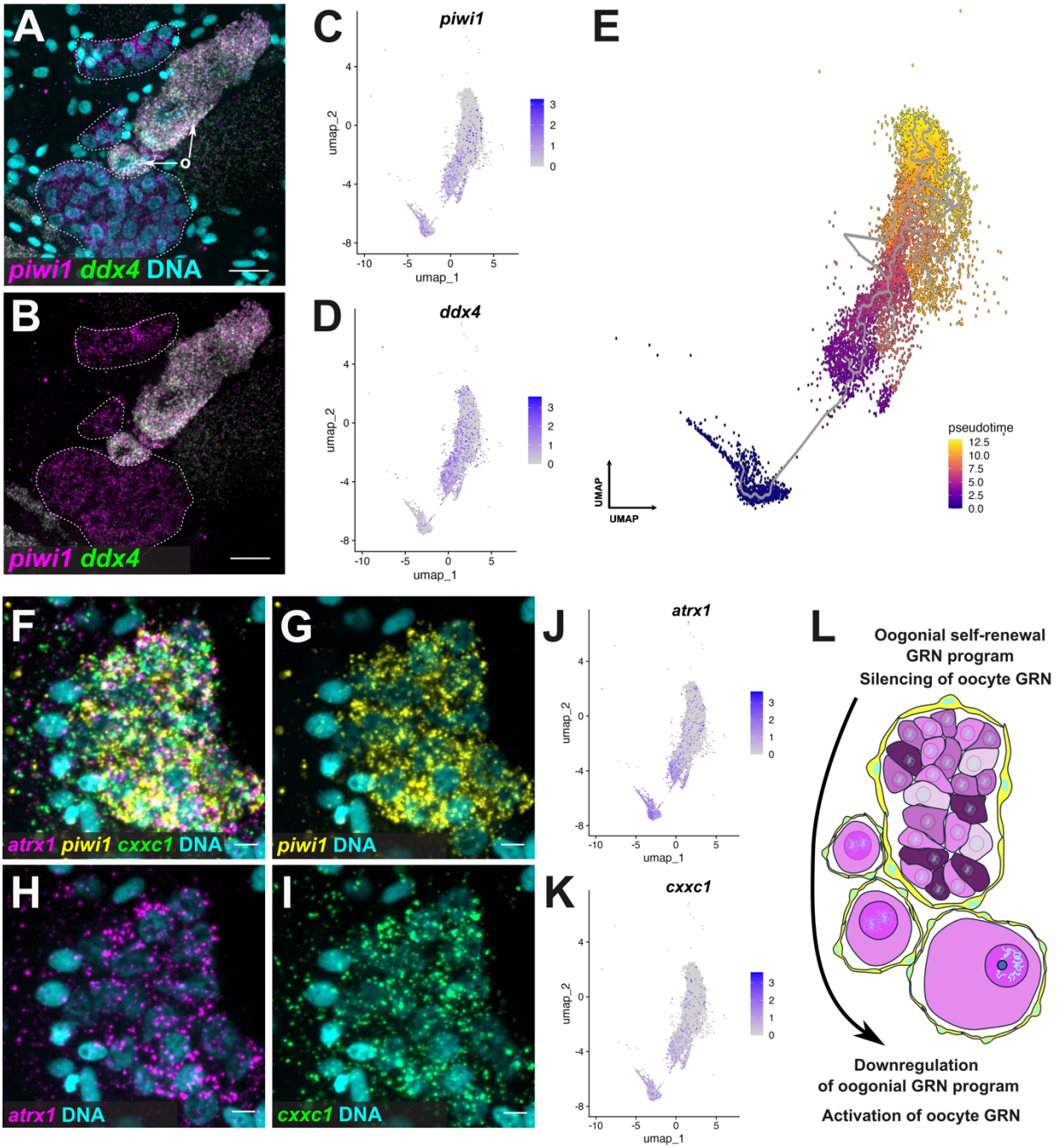

Figure 5. Reconstruction of the early oogenesis developmental trajectory. (A-B) HCR for the germline markers *piwi1* and *ddx4* highlights the absence of *ddx4* in the germ cell cysts. Dotted lines outline the germ cell cyst. Nuclei were labelled with DAPI (cyan). **(C-D)** Feature plot showing the expression levels of *piwi1* and *ddx4* along the germline clusters of the *P. miniata* single cell atlas. **(E)** UMAP depicting the developmental trajectory of the germline clusters reconstructed with Monocle3. The germ cell cluster 13 has been used as a root. **(F-I)** HCR for the transcriptional regulators *atrx1* and *cxxc1* paired with *piwi1* confirms their expression in germ cell cysts. Scale bars are 5 µm. **(J-K)** Feature plot showing the distribution

502 of *atrx1* and *cxxc1* transcripts along the trajectory confirms their differential expression in clusters
503 corresponding to germ cell cysts. Nuclei were labelled with DAPI (cyan). **(L)** Cartoon highlighting the
504 difference in gene expression of the oogonia in the germ cell cysts versus the oocyte stages. o, oocytes.
505

506 **Signaling pathways across ovarian cell types**

507 What are the major signaling pathways that could control oogenesis and folliculogenesis?
508 We first mined our atlas for the expression of gene groups corresponding to either ligands
509 or downstream signaling cascades of the Wnt, Tgfb, Delta/Notch, Hh, and RA signaling
510 pathways (**Fig. 6A, S8A**).We found that the clusters that most strongly express Wnt ligands
511 correspond to epithelium, oocytes and immune cells, while follicle I, germ, oocytes,
512 neurons and muscles are able to respond to the signal based on the expression of frizzled
513 receptors, *dvl3, gsk3, apc, tcf/Lef* and *β-catenin* (**Fig. 6A, S8A**). Similarly, Tgfβ ligands are
514 expressed by the epithelium, follicle I, follicle III and muscle clusters, while their receptors
515 and signaling cascade factors are expressed in germ, oocytes, muscles, follicle III and
516 immune cells (**Fig. 6A, S8A**). For Delta/Notch signaling, *delta* transcripts are found in
517 epithelial, follicle II, follicle III and oocytes cell type groups, and the signal is predicted to
518 be received by follicle I, oocytes and neurons *notch* receptors and gamma secretase
519 subunits (**Fig. 6A, S8A**). Hedgehog (*hh*) is exclusively expressed by neurons, and the
520 signal may be received by follicle I and germ cell type groups based on the expression of
521 patched and smoothened receptors (**Fig. 6A, S8A**). Lastly, retinoic acid synthesis
522 machinery gene orthologs, including *sdr7, aldh1, aldh3* and *aldh8* are differentially
523 expressed in the follicle II, germ, and oocyte cell groups, and the cells that express RA
524 receptors *rar, rxr* and *ppar* belong to the follicle I, III, germ, neural and muscle ones (**Fig.
525 6A, S8A**). Degradation of RA is performed by cells expressing *cyp26,* which includes the
526 follicle I group, while its transport is mediated by cells that express *fabpl3,* which includes
527 the follicle I and follicle II groups (**Fig. 6A, S8A**). Our results indicate the presence of a
528 complex signaling system involved in sea star oogenesis by which diverse signals are
529 produced and received both by the follicle cells, the cells of the germ lineage, and the
530 ovarian neurons.
531

532 We next focused on Tgfβ signaling, which has been implicated in primordial germ cell
533 development and follicular growth in mammals (1,70,71) (**Fig. 6C-F, S8B-D**). Our atlas

indicates that Tgfβ signaling may be active within the oocyte-follicle complex. Of the genes tested, only *tgfb2* ligand was uniquely expressed in somatic tissues and primarily in follicle cells enwrapping the oogonia and mature oocytes (**Fig. 6C**). We found Tgfβ receptors *tgfbr3*, *alk2* and the intercellular messenger *smad5* expressed by both the germ cell cysts and developing oocytes, validating the scRNA-seq predictions (**Fig. 6D-F**). In addition, our atlas showed that several Bmp ligands are expressed within the germ lineage, suggesting that Tgfβ signaling may also be active between growing oocytes, or acting upon follicle cells, a dual role also reported in mammals (**Fig. 6A, S8A**). HCR for *bmp1* and *bmp4* confirmed these predicted expression patterns (**Fig. S8B-D**). In summary, our results support the deep evolutionary conservation of Tgfβ signaling pathway components within the ovarian follicle.

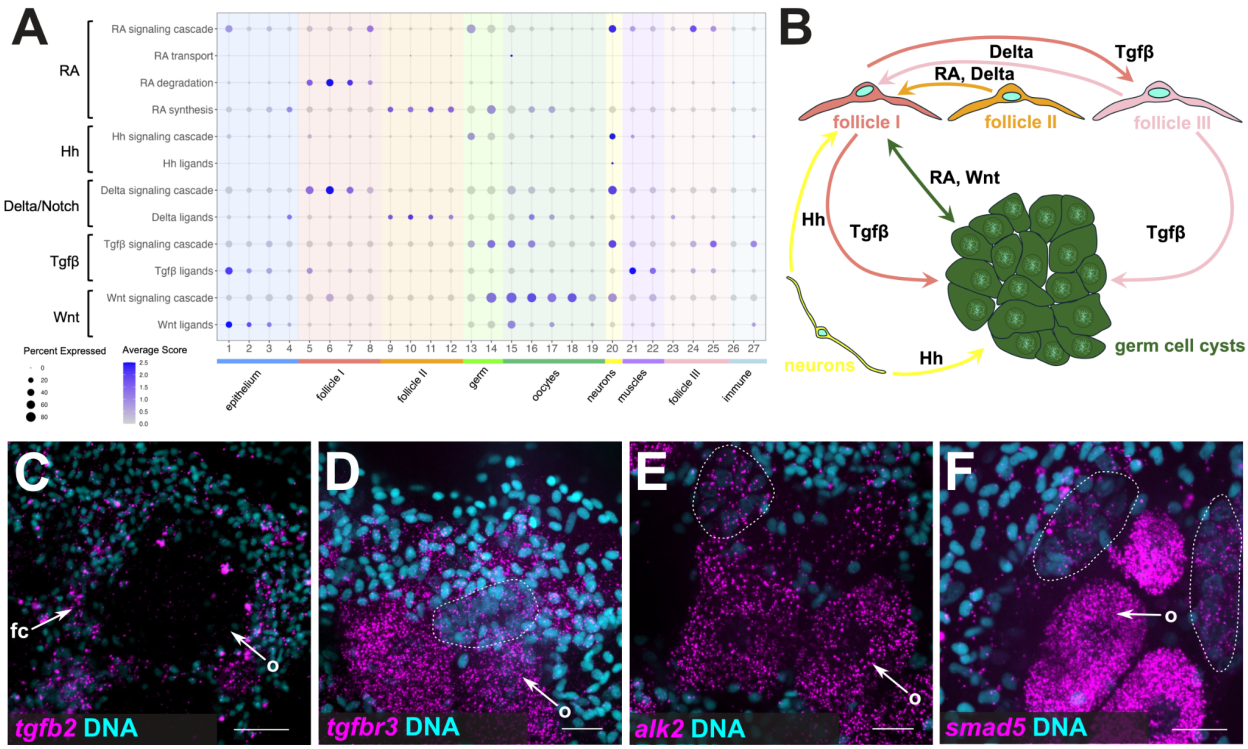

Figure 6. Putative signaling pathways involved in ovarian cell type crosstalk. (A) Dotplot showing the average score of gene groups corresponding to ligands and signaling cascade genes in relation to Wnt, Tgfβ, Delta/Notch, Hh and RA signaling pathways across the *P. miniata* ovarian cell type groups. (**B**) Schematic representation of the predicted paracrine crosstalk between follicle cells, neurons and germ cell cysts. (**C**) HCR for *tgfb2* labeling follicle cells. Scale bar is 40 µm. (**D-F**) HCRs for *tgfbr3*, *alk2* and *smad5* show localization within the germ cell cysts and oocytes spatially confirming the scRNA-seq predictions.

553 Scale bar is 20 µm. Dotted lines outline the germ cell cysts. Nuclei were labelled with DAPI (cyan). fc, follicle
554 cells; o, oocytes.
555

556 **Evidence for pre-chordate origins of the HPG axis**

557 Vertebrate oogenesis is regulated by endocrine signaling between the hypothalamus, the
558 pituitary gland, and the ovary. Therefore, we asked how the ovarian nervous system might
559 serve as an intrinsic paracrine regulator of oogenesis. We found that most neuropeptide
560 synthesis genes are specifically expressed by neuronal cluster 20, including, tryptophan
561 hydroxylase (*tph*), tyrosine hydroxylase (*th*), choline O-acetyltransferase (*chat*), histidine
562 decarboxylase (*hdc*), and glutamate decarboxylase (*gad*) are expressed , indicating
563 serotonergic, dopaminergic, cholinergic, histaminergic and GABAergic neurons,
564 respectively (**Fig. S9A**) (72,73). Moreover, we found that sixteen different neuropeptides
565 are expressed in the same cell cluster (**Fig. S9A**). Immunofluorescence for TH and
566 serotonin (5HT) confirmed the presence of extensive dopaminergic and serotonergic
567 neuronal subepidermal networks respectively (**Fig. S9C-D'**). To our surprise, we also
568 detected serotonin within the germ cell cysts, (**Fig. 7A-B**) as well as genes encoding for
569 neuromodulators and neuropeptides including *tph*, *chat*, prolactin-releasing peptide
570 (*prrp*), luqin (*lqp*) and uncharacterized neuropeptide precursor (*np25*) (**Fig. S9A**). The
571 widespread presence of neuromodulators within the germ cell cysts prompted us to
572 further assess the link between ovarian neurons and germ cell cysts (**Fig. 7C**).
573 Importantly, most of the ligand/receptor pairs used for this analysis have been previously
574 identified and some even de-orphanized in sea stars and sea urchins (74–80). We found
575 that neuropeptides involved in the function and regulation of the mammalian HPG axis,
576 including gonadotropin-releasing hormone (*gnrh*), kisspeptin (*kpp*), *oxy/vp* (81) and the
577 echinoderm muscle relaxant neuropeptide F-Salmf (76) were specifically expressed in
578 the neuron cell type group and in both germ cell groups (**Fig. 7C**). Their receptors were
579 predominantly expressed in the germ cell cyst clusters, suggesting crosstalk between
580 neurons and germ cell cysts (**Fig. S7C**). Similarly, the receptors for serotonin, dopamine
581 and GABA were found expressed within the germ cell cyst clusters (**Fig. S9B**). On the
582 other hand, we found the ngffyamide (*ngffap*) neuropeptide to be expressed primarily in
583 the germ and oocytes cell type groups and not in the neurons, while the latter contained
584 transcripts for its receptor (**Fig. S7C**). Moreover, we also found neuropeptides including

585 *prrp* and *lqp* as well as their receptors expressed by both germ cell cysts and neurons
586 (**Fig. S7C**). Last, we report additional putative neuropeptidergic crosstalk of the ovarian
587 neurons with the muscles and the ovarian epithelium (**Fig. S7C**).

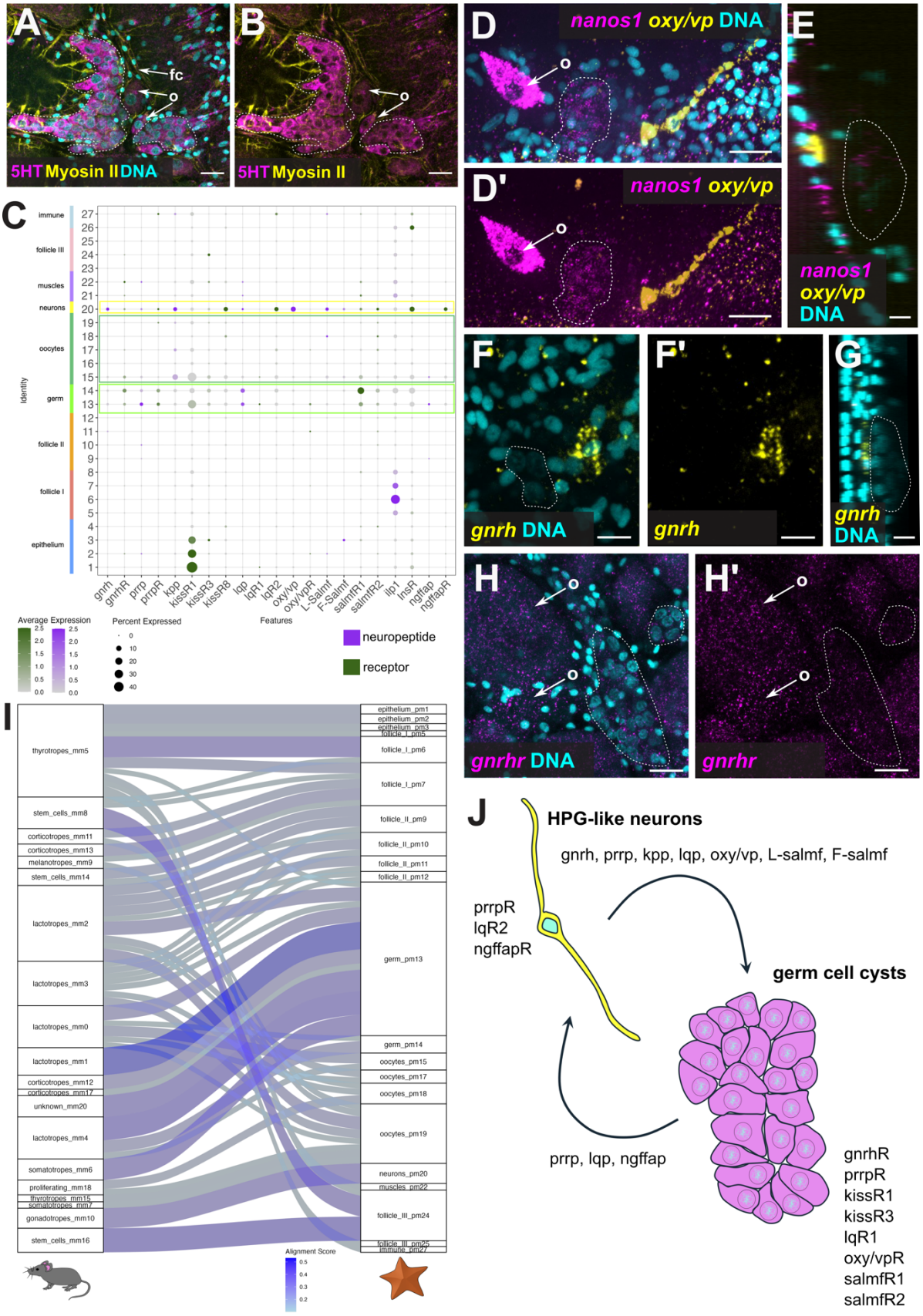
A
fc
o
5HT Myosin II DNA
B
o
5HT Myosin II
C
immune
follicle III
muscles
neurons
oocytes
germ
follicle II
follicle I
epithelium
Identity
gnrh
gnrhR
prrp
prrpR
kpp
kissR1
kissR3
kissR8
lqp
lqR1
lqR2
oxy/vp
oxy/vpR
L-Salmf
F-Salmf
salmfR1
salmfR2
ilp1
insR
ngffap
ngffapR
Features
Average Expression
Percent Expressed
neuropeptide
receptor
D
nanos1 oxy/vp DNA
o
D'
nanos1 oxy/vp
o
E
nanos1
oxy/vp
DNA
F
gnrh DNA
F'
gnrh
G
gnrh
DNA
H
o
o
gnrhr DNA
H'
o
o
gnrhr
I
thyrotropes_mm5
stem_cells_mm8
corticotropes_mm11
corticotropes_mm13
melanotropes_mm9
stem_cells_mm14
lactotropes_mm2
lactotropes_mm3
lactotropes_mm0
lactotropes_mm1
corticotropes_mm12
corticotropes_mm17
unknown_mm20
lactotropes_mm4
somatotropes_mm6
proliferating_mm18
thyrotropes_mm15
somatotropes_mm7
gonadotropes_mm10
stem_cells_mm16
epithelium_pm1
epithelium_pm2
epithelium_pm3
follicle_I_pm5
follicle_I_pm6
follicle_I_pm7
follicle_II_pm9
follicle_II_pm10
follicle_II_pm11
follicle_II_pm12
germ_pm13
germ_pm14
oocytes_pm15
oocytes_pm17
oocytes_pm18
oocytes_pm19
neurons_pm20
muscles_pm22
follicle_III_pm24
follicle_III_pm25
immune_pm27
Alignment Score
J
HPG-like neurons
gnrh, prrp, kpp, lqp, oxy/vp, L-salmf, F-salmf
prrpR
lqR2
ngffapR
germ cell cysts
prrp, lqp, ngffap
gnrhR
prrpR
kissR1
kissR3
lqR1
oxy/vpR
salmfR1
salmfR2

588

589 **Figure 7. Neuropeptidergic profile of the *P. miniata* intrinsic ovarian nervous system. (A-B)**
590 Immunofluorescence of 5HT and Myosin II. Dotted lines outline the germ cell cysts. Scale bars 20 µm. **(C)**
591 Dotplot showing the average expression of the reconstructed and/or deorphanized pairs of
592 neuropeptides/receptors. **(D-D')** HCR for *oxy/vp* and *nanos1* shows the relatively short distance between
593 the oxy/vp positive neurons and the germ cell cysts. Scale bars in panels are 20 µm. Dotted lines outline
594 the germ cell cysts. **(E)** Orthogonal views of the *oxy/vp* and *nanos1* HCR, shows the close proximity of the
595 *oxy/vp* neuron in respect to the *nanos1* positive germ cell cysts. Dotted lines outline the germ cell cysts.
596 Scale bar is 10 µm. **(F-F')** HCR for *gnrh* in subepithelial ovarian neurons. Scale bars in panels are 20 µm.
597 Dotted lines outline the germ cell cysts. **(G)** Orthogonal views of a *gnrh* HCR, highlights the spatial
598 organization of the *gnrh* positive neurons in close proximity to the germ cell cysts. Scale bar is 10 µm.
599 Dotted lines outline the germ cell cysts. **(H-H')** HCR for *gnrhr* confirms the single cell predictions of
600 expression in the germ lineage. Scale bars are 20 µm. Dotted lines outline the germ cell cysts. **(I)** Sankey
601 plot depicting the alignment scores between adult sea star ovarian cell atlas with the adult mouse pituitary
602 gland one. **(J)** Schematic representation of the components participating in the predicted crosstalk between
603 the intrinsic ovarian neurons and the germ cell cysts. Nuclei are labelled with DAPI (cyan). fc, follicle cells;
604 o, oocytes.
605
606 To test these predictions, we examined expression of *oxy/vp* as well as for the lowly
607 expressed *gnrh* and *gnrhr*. Using HCR, we found that oxy/vp are expressed exclusively
608 in rare subepidermal neurons (1-2 per ovarian lobe, **Fig. 7D-D', S9 E-E'**). These *oxy/vp*
609 positive neurons were in close proximity to the germ cell cysts, suggesting potential
610 crosstalk (**Fig. 7E**). Similarly, we detected *gnrh*+ cells in proximity to germ cell cysts, while
611 *gnrhr* was expressed both in the cysts and oocytes (**Fig. 7F-H'**). Previous studies in the
612 adult sea star *A. rubens* reported that *gnrh* is expressed predominantly within the sea
613 star's nervous system (oral nerve ring and radial nerve cords). Consistent with this prior
614 work, and supporting the specificity of our HCR probes, *gnrh* and *gnrhr* were in
615 complementary regions of the oral nerve ring and the radial nerve cord (**Fig. S9F-F'**).
616
617 Taken together, our analysis found that many known hypothalamic neuromodulators
618 involved in the vertebrate HPG axis such as 5HT, dopamine, GABA, GNRH, KPP and
619 OXY/VP (81) as well as the pituitary gland secreted PrRP (82) are all present in the sea
620 star ovarian neurons. To further test if such a system is in place in sea star ovaries, we
621 assessed the similarity between sea star cell type families with the mammalian pituitary
622 gland using SAMap (**Fig. 7I**). Surprisingly, this analysis showed that the sea star neurons

623 exclusively align with pituitary gland gonadotropes, which upon stimulation by
624 hypothalamic *gnrh* produce the gonadotropins that control sex hormone production,
625 oogenesis, and ovulation in mammals (83). Our comparison showed alignments between
626 pituitary gland thyrotropes with the sea star follicle cells (follicle I) while the germ cell cysts
627 aligned with the pituitary gland lactotropes (**Fig. 7I**). Altogether, our results reveal a
628 diverse and putatively multifunctional intrinsic ovarian nervous system that may
629 communicate with the germ cell cysts (**Fig. 7J**). Lastly, our data suggest that the sea star
630 ovarian nervous system has a dual hypothalamic-like and gonadotropic-like state that
631 could act as a localized HPG-like center operating in parallel or independently from the
632 oral nerve ring and radial nerve cords to regulate sea star oogenesis, oocyte maturation
633 and spawning behavior.
634

635 **Discussion**

636 Sexual reproduction depends on the interactions between multiple cell types within the
637 ovary. Ovarian structure varies across animals, reflecting differences in reproductive
638 strategies and adaptations to different environments. For instance, many marine
639 invertebrates follow seasonal patterns and release large quantities of gametes into the
640 water column, whereas in mammals seasonal mating patterns result in the fertilization of
641 only a limited number of oocytes within the oviduct. Despite these differences, in most
642 animals studied, the ovary serves two critical roles as both an endocrine organ that
643 produces steroid hormones, and as the niche for oocyte development. Here we took
644 advantage of the easily accessible, optically transparent and highly fecund sea star ovary,
645 representing an extreme case of reproductive output, to explore the identity and the
646 evolutionary origins of the ovarian cell types in a non-chordate deuterostome. Our single
647 cell atlas identified nine cell type groups distributed across twenty-seven transcriptionally
648 distinct clusters which we then spatially mapped within the ovary. We show that the ovary
649 is made of seven somatic cell groups corresponding to ciliated epithelium, neurons,
650 muscles, immune cells and three different types of follicle cells, corroborating previous
651 morphological studies (36). We also found cell groups corresponding to young oocytes
652 as well as proliferating germ cells organized into cysts. Single cell trajectory analysis finds
653 connections between the cysts and the oocytes and shows how the gene expression

654 changes during early oogenesis. Collectively, this analysis provides a framework for
655 understanding echinoderm oogenesis at a new depth, and a valuable resource for future
656 investigation of reproductive biology and cell type evolution.
657

658 **Sea star follicle cells are a heterotypic group**

659 Follicle cells that enwrap oocytes serve important roles in oogenesis across animals (84).
660 In insects, different types of follicle cells produce yolk components or contribute to the
661 formation of egg protective layers (85). In mammals and fish, granulosa cells are involved
662 in the production of estrogen, nutrient transfer and regulation of oocyte maturation
663 (1,86,87). Theca cells instead populate the outer layers of the follicle and produce steroid
664 hormones that are taken up and converted to estrogen by granulosa cells. Similarly in
665 echinoderms, follicle cells produce maturation-inducing molecules, such as 1-
666 methyladenine in sea stars, upon stimulation by the gonad stimulating substance (GSS)
667 from the nervous system that triggers the resumption of meiosis in arrested oocytes
668 (88,89). However, the molecular signature of follicle cells has not been well defined. Here
669 we provide evidence for three diversified sea star follicle cell groups, one that appears to
670 be echinoderm specific (follicle II), involved primarily in vitellogenesis, and two that
671 express genes typically found in granulosa (follicle I) and theca cells (follicle III) in
672 mammals. Surprisingly, our results suggest possible pre-chordate evolutionary origins for
673 theca and granulosa cells.

674 In support of this hypothesis, our transcriptomic and spatial analysis discovered that
675 several genes associated with mammalian granulosa cells are also expressed by a
676 subset of sea star follicle cells. This includes the transcription factors *foxl2* and *gata4*, and
677 the protein hormone inhibin beta (*inhbb*) (1,44). The forkhead transcription factor *foxl2* is
678 a crucial member of the GRN controlling the granulosa cell proliferation and differentiation
679 in mammals (43), and in sea stars we find it expressed by a subset of follicle cells that
680 are in direct contact with the developing oocytes. In addition, we detected primary cilia on
681 the surface of the follicle cells enwrapping oocytes, which is a conserved feature of
682 estrogen-producing granulosa cells of antral follicles in mice (90). Our cross-species
683 analysis revealed that a granulosa-like cell cluster (follicle I) consistently aligned with
684 granulosa cell clusters in humans and mice, and with follicle cells in the rest of the species

analyzed. This raises the possibility that sea star granulosa cells influence follicle development through similar mechanisms as in mammals. For instance, in mammals granulosa cells secrete several Tgfβ family ligands that influence oocyte development (91). Similarly, we find that such ligands are expressed by the granulosa-like (follicle) cells. Last, our scRNA-seq data suggest that sea star granulosa-like cells produce and respond to RA signaling, which prior work has been found to regulate granulosa cell proliferation and steroidogenesis in mammals (92). Moreover, our data show that the follicle III cell group expresses star and *cyp17a1*, genes essential for steroidogenesis in mammalian theca cells. The sea star ovarian epithelium shares similarities with theca cells in zebrafish, mouse, and fetal human ovaries, with two clusters expressing *cyp17a1* and one expressing star, indicating a potential role in steroid hormone production similar to what was previously reported in humans (93). Taken together our data suggest that the sea star ovary harbors follicle cell types evolutionarily conserved to distinct follicle cell populations in other deuterostomes as well as protostomes.

Molecular identification of putative oogonial stem cells

An evolutionarily conserved feature of oogenesis is the formation of germ cell cysts. Clusters of cytoplasmically interconnected oogonia have been found in the ovaries of a variety of animals including insects, amphibians, reptiles, birds, and mammals (35,94–99). Here we define the germline identity of sea star germ cell nests and provide evidence for intercellular bridges within them, thus suggesting that germ cell cysts are conserved in non-chordate deuterostomes. Using 3D segmentation and reconstruction, we also defined the spatial organization of oogenesis, in which germ cell cysts are localized to the periphery of the ovarian lobe along with young oocytes organized in primary follicles. Cyst expressed genes include the conserved germline markers *piwi1*, *nanos1*, *nanos3*, *boll*, *msl3*, meiotic recombination components *sycp1* and *mlh1*, and transcriptional regulators including *figla*, *atrx1* and *cxxc1* (59,100–102). We also detect cell proliferation within the cysts, supporting them as the likely source of new oogonia and oocytes in the adult ovary (103). The conserved germline RNA helicase *ddx4/vasa* is inactive in the cysts, but is expressed in early follicles, similar to what was shown in marsupial fetal germ cells (104-

715 106). This repression may contribute to maintaining an undifferentiated state, as seen in
716 fruit flies where *ddx4* knockout led to arrested oocyte development (107). Additionally, we
717 hypothesize that the self-renewal-meiotic entry decision could be regulated by RA, Wnt,
718 Tgfβ and Hh pathways, whose respective receptors and intracellular components were
719 found expressed in the germ cell cysts. These results support an ancient role for these
720 pathways in oogenesis, as demonstrated in other species including mice and amphibians
721 (108–111).

722

723 **Neuronal control of oogenesis predates the establishment of chordate HPG axis**

724 Oogenesis and ovulation are regulated by neuroendocrine signals from the nervous
725 system in many animals. In vertebrates, this signaling occurs between the hypothalamus,
726 the pituitary gland, and the gonad, also known as the HPG axis. HPG signaling molecules
727 include neuropeptides *gnrh* and *oxy/vp* that are secreted by the hypothalamus and
728 received by gonadotropin cells within the pituitary gland. This induces the secretion of the
729 gonadotropin hormones follicle stimulating hormone (FSH) and luteinizing hormone (LH),
730 that in turn regulate gametogenesis within the gonad through activation of the
731 steroidogenic pathway. In mammals, the secretion of upstream hypothalamic
732 neuropeptides is regulated by several neuromodulators including 5HT, dopamine, GABA,
733 PrRP and KPP (112–116). How might oogenesis and ovulation be regulated in animals
734 like sea stars that lack a central nervous system?

735 Foundational work in sea stars found that soluble signals from radial nerves induce oocyte
736 maturation and spawning, indicating that oogenesis is under neural control even in
737 invertebrates (117). Our data further argue that the sea star ovary itself contains an
738 intrinsic neurochemical regulatory system. For instance, we found that the epithelium,
739 germ cells, and oocytes produce previously identified neuropeptides such as *rgpp* and
740 *trh*, both of which have been found to be produced by the radial nerve cords and regulate
741 oogenesis in echinoderms (118,119). We also found numerous other HPG-associated
742 signaling factors, including 5HT, dopamine, GABA, KPP, GNRH, PrRP and OXY/VP to
743 be expressed in the intrinsic ovarian nerve plexus and their respective receptors in the
744 germ cell cysts. Strikingly, our data suggest the presence of a novel echinoderm ovarian

745 cell type that features a dual molecular identity resembling chordate hypothalamic
746 neurons and pituitary gonadotropic endocrine cells. In support of this is the similarity of
747 the sea star neuronal cluster with the one corresponding to the mouse pituitary gland
748 gonadotropes.

749 Taken together our analysis provides molecular evidence towards the presence of a
750 hypothalamic-like and gonadotropic-like intrinsic ovarian neuroendocrine signaling
751 system in non-chordate deuterostomes. We hypothesize that the echinoderm ovarian
752 neurons are analogous to the mammalian HPG axis elements. We speculate that during
753 animal evolution, oogenesis was initially regulated by intrinsic neuroendocrine systems
754 within the ovary and as organisms became more complex the regulatory role was co-
755 opted by distinct organs such as complex interconnected nervous systems and endocrine
756 glands.

757

758 **Acknowledgements**

759 We thank Jamie MacKinnon, Akshay Kane, Beverly Naigles and Karen Velez, current
760 and past members of the Swartz lab, for advice and fruitful discussions throughout the
761 duration of this project. We thank Maria Ina Arnone (Stazione Zoologica Anton Dohrn) for
762 helping by providing the 1e11 and Mhc antibodies, and *S. purpuratus* ovaries. We also
763 thank Rossella Annunziata (Stazione Zoologica Anton Dohrn) for kindly providing us with
764 *H. tubulosa* ovaries. We would also like to thank Louie Kerr, the Central Microscopy
765 Facility at the Marine Biological Laboratory (Woods Hole, MA, USA) and Chris Bjornsson
766 (ZEISS), for imaging assistance with confocal microscopy. We are grateful to Lisa Abbo
767 and the Marine Resources Center staff for providing excellent animal care and husbandry
768 of adult *P. miniata* used in this work.

769

770 **Funding**

771 This work was supported by the National Institutes of Health (R00HD099315 to S.Z.S.)
772 and by a Faculty Recruitment Gift from the Hibbitt Foundation. P.P. was supported by a
773 Postdoctoral fellowship awarded by the Global Consortium for Productive Health

(previously known as Global Consortium for Reproductive Longevity and Equality) part of the Buck Center for Healthy Aging in Women.

Competing interests

The authors declare no competing interests.

Author contributions

Conceptualization: P.P., S.Z.S.; Methodology: P.P., S.Z.S.; Formal analysis: P.P., C.W., D.V.; Investigation: P.P., S.Z.S.; Writing - original draft: P.P.; Writing - review & editing: P.P., C.W., D.V., S.Z.S.; Visualization: P.P., C.W.; Supervision: S.Z.S.; Project administration: S.Z.S.; Funding acquisition: S.Z.S.

References

1. Prasasya RD, Mayo KE. Regulation of follicle formation and development by ovarian signaling pathways. In: The Ovary. Elsevier; 2019. p. 23–49.

2. Orisaka M, Tajima K, Tsang BK, Kotsuji F. Oocyte-granulosa-theca cell interactions during preantral follicular development. J Ovarian Res. 2009 Jul 9;2(1):9.

3. Tsukamura H. Kobayashi Award 2019: The neuroendocrine regulation of the mammalian reproduction. Gen Comp Endocrinol. 2022 Jan 1;315(113755):113755.

4. Grive KJ, Freiman RN. The developmental origins of the mammalian ovarian reserve. Development. 2015 Aug 1;142(15):2554–63.

5. Packer C, Tatar M, Collins A. Reproductive cessation in female mammals. Nature. 1998 Apr 23;392(6678):807–11.

6. Armstrong AR, Drummond-Barbosa D. Insulin signaling acts in adult adipocytes via GSK-3β and independently of FOXO to control Drosophila female germline stem cell numbers. Dev Biol. 2018 Aug 1;440(1):31–9.

7. Juliano CE, Swartz SZ, Wessel GM. A conserved germline multipotency program. Development. 2010 Dec;137(24):4113–26.

8. Arnone MI, Byrne M, Martinez P. Echinodermata. In: Evolutionary Developmental Biology of Invertebrates 6. Vienna: Springer Vienna; 2015. p. 1–58.

9. Bodnar AG. Marine invertebrates as models for aging research. Exp Gerontol. 2009 Aug;44(8):477–84.

10. Ernst SG. Offerings from an urchin. Dev Biol. 2011 Oct 15;358(2):285–94.

11. Arnone MI, Andrikou C, Annunziata R. Echinoderm systems for gene regulatory studies in evolution and development. Curr Opin Genet Dev. 2016 Aug;39:129–37.

12. Swartz SZ, McKay LS, Su KC, Bury L, Padeganeh A, Maddox PS, et al. Quiescent cells actively replenish CENP-A nucleosomes to maintain centromere identity and proliferative potential. Dev Cell. 2019 Oct 7;51(1):35–48.e7.

13. Paganos P, Voronov D, Musser JM, Arendt D, Arnone MI. Single-cell RNA sequencing of the Strongylocentrotus purpuratus larva reveals the blueprint of major cell types and nervous system of a non-chordate deuterostome. Elife. 2021 Nov 25;10.

14. Magri MS, Voronov D, Foley S, Martínez-García PM, Franke M, Cary GA, et al. Deep conservation of cis-regulatory elements and chromatin organization in echinoderms uncover ancestral regulatory features of animal genomes. bioRxiv. 2024.

15. Dainat J, Hereñú D, Murray KD, Davis E, Ugrin I, Crouch K, et al. NBISweden/AGAT: AGAT-v1.4.1. Zenodo. 2024.

16. Zheng GXY, Terry JM, Belgrader P, Ryvkin P, Bent ZW, Wilson R, et al. Massively parallel digital transcriptional profiling of single cells. Nat Commun. 2017 Jan 16;8(1):14049.

17. Hao Y, Stuart T, Kowalski MH, Choudhary S, Hoffman P, Hartman A, et al. Dictionary learning for integrative, multimodal and scalable single-cell analysis. Nat Biotechnol. 2024 Feb;42(2):293–304.

18. Chitiashvili T, Dror I, Kim R, Hsu FM, Chaudhari R, Pandolfi E, et al. Female human primordial germ cells display X-chromosome dosage compensation despite the absence of X-inactivation. Nat Cell Biol. 2020 Dec;22(12):1436–46.

19. Isola JVV, Ocañas SR, Hubbart CR, Ko S, Mondal SA, Hense JD, et al. A single-cell atlas of the aging mouse ovary. Nat Aging. 2024 Jan;4(1):145–62.

20. Liu Y, Kossack ME, McFaul ME, Christensen LN, Siebert S, Wyatt SR, et al. Single-cell transcriptome reveals insights into the development and function of the zebrafish ovary. Elife. 2022 May 19;11:e76014.

21. Oulhen N, Morita S, Pieplow C, Onorato TM, Foster S, Wessel G. Conservation and contrast in cell states of echinoderm ovaries. Mol Reprod Dev. 2024 Aug;91(8):e23721.

22. Rust K, Byrnes LE, Yu KS, Park JS, Sneddon JB, Tward AD, et al. A single-cell atlas and lineage analysis of the adult Drosophila ovary. Nat Commun. 2020 Nov 6;11(1):5628.

23. Allensworth-James M, Banik J, Odle A, Hardy L, Lagasse A, Moreira ARS, et al. Control of the anterior pituitary cell lineage regulator POU1F1 by the stem cell determinant Musashi. Endocrinology. 2021 Mar 1;162(3):bqaa245.

24. Tarashansky AJ, Musser JM, Khariton M, Li P, Arendt D, Quake SR, et al. Mapping single-cell atlases throughout Metazoa unravels cell type evolution. Elife. 2021 May 4;10:e66747.

25. Piovani L, Leite DJ, Yañez Guerra LA, Simpson F, Musser JM, Salvador-Martínez I, et al. Single-cell atlases of two lophotrochozoan larvae highlight their complex evolutionary histories. Sci Adv. 2023 Aug 2;9(31):eadg6034.

26. Cao J, Spielmann M, Qiu X, Huang X, Ibrahim DM, Hill AJ, et al. The single-cell transcriptional landscape of mammalian organogenesis. Nature. 2019 Feb;566(7745):496–502.

27. Hörl D, Rojas Rusak F, Preusser F, Tillberg P, Randel N, Chhetri RK, et al. BigStitcher: reconstructing high-resolution image datasets of cleared and expanded samples. Nat Methods. 2019 Sep;16(9):870–4.

28. Formery L, Peluso P, Kohnle I, Malnick J, Thompson JR, Pitel M, et al. Molecular evidence of anteroposterior patterning in adult echinoderms. Nature. 2023 Nov;623(7987):555–61.

29. Kuehn E, Clausen DS, Null RW, Metzger BM, Willis AD, Özpolat BD. Segment number threshold determines juvenile onset of germline cluster expansion in Platynereis dumerilii. J Exp Zool B Mol Dev Evol. 2022 Jun;338(4):225–40.

30. Paganos P, Caccavale F, La Vecchia C, D'Aniello E, D'Aniello S, Arnone MI. FISH for all: A fast and efficient fluorescent in situ hybridization (FISH) protocol for marine embryos and larvae. Front Physiol. 2022 Apr 19;13:878062.

31. Perillo M, Paganos P, Spurrell M, Arnone MI, Wessel GM. Methodology for whole mount and fluorescent RNA in situ hybridization in echinoderms: Single, double, and beyond. In: Methods in Molecular Biology. New York, NY: Springer US; 2021. p. 195–216. (Methods in molecular biology (Clifton, N.J.)).

32. Ćorić A, Stockinger AW, Schaffer P, Roković D, Tessmar-Raible K, Raible F. A fast and versatile method for simultaneous HCR, immunohistochemistry and Edu labeling (SHInE). Integr Comp Biol. 2023 Aug 23;63(2):372–81.

33. Mita M, Osugi T, Takahashi T, Watanabe T, Satake H. Mechanism of gamete shedding in starfish: Involvement of acetylcholine in extracellular Ca2+-dependent contraction of gonadal walls. Gen Comp Endocrinol. 2020 May

876 1;290(113401):113401.

877 34. Zickler D, Kleckner N. The leptotene-zygotene transition of meiosis. Annu Rev
878 Genet. 1998;32:619–97.

879 35. Pepling ME. From primordial germ cell to primordial follicle: mammalian female
880 germ cell development. Genesis. 2006 Dec;44(12):622–32.

881 36. Schoenmakers HJ, Colenbrander PH, Peute J, van Oordt PG. Anatomy of the
882 ovaries of the starfish Asterias rubens (Echinodermata). A histological and
883 ultrastructural study. Cell Tissue Res. 1981;217(3):577–97.

884 37. Fresques T, Swartz SZ, Juliano C, Morino Y, Kikuchi M, Akasaka K, et al. The
885 diversity of nanos expression in echinoderm embryos supports different
886 mechanisms in germ cell specification. Evol Dev. 2016 Jul;18(4):267–78.

887 38. Reich A, Dunn C, Akasaka K, Wessel G. Phylogenomic analyses of Echinodermata
888 support the sister groups of Asterozoa and Echinozoa. PLoS One. 2015 Mar
889 20;10(3):e0119627.

890 39. Zazueta-Novoa V, Onorato TM, Reyes G, Oulhen N, Wessel GM. Complexity of
891 yolk proteins and their dynamics in the sea star Patiria miniata. Biol Bull. 2016
892 Jun;230(3):209–19.

893 40. Xia L, Yin GL, Long Y, Sun F, Wang BB, Zhu Y, et al. Essential role of CFAP77-
894 CCDC105-TEX43 subcomplex in connecting axonemal A and B tubules for
895 mammalian sperm motility. Cell Biology. bioRxiv. 2025.

896 41. Fan X, Bialecka M, Moustakas I, Lam E, Torrens-Juaneda V, Borggreven NV, et al.
897 Single-cell reconstruction of follicular remodeling in the human adult ovary. Nat
898 Commun. 2019 Jul 18;10(1):3164.

899 42. Juengel JL, Bibby AH, Reader KL, Lun S, Quirke LD, Haydon LJ, et al. The role of
900 transforming growth factor-beta (TGF-beta) during ovarian follicular development in
901 sheep. Reprod Biol Endocrinol. 2004 Nov 25;2(1):78.

902 43. Pisarska MD, Barlow G, Kuo FT. Minireview: roles of the forkhead transcription
903 factor FOXL2 in granulosa cell biology and pathology. Endocrinology. 2011
904 Apr;152(4):1199–208.

905 44. Bennett J, Baumgarten SC, Stocco C. GATA4 and GATA6 silencing in ovarian
906 granulosa cells affects levels of mRNAs involved in steroidogenesis, extracellular
907 structure organization, IGF-I activity, and apoptosis. Endocrinology. 2013
908 Dec;154(12):4845–58.

909 45. Liu Z, Castrillon DH, Zhou W, Richards JS. FOXO1/3 depletion in granulosa cells
910 alters follicle growth, death and regulation of pituitary FSH. Mol Endocrinol. 2013
911 Feb;27(2):238–52.

46. Vos MC, van der Wurff AA, Last JTJ, de Boed EAM, Smeenk JMJ, van Kuppevelt TH, et al. Immunohistochemical expression of MMP-14 and MMP-2, and MMP-2 activity during human ovarian follicular development. Reprod Biol Endocrinol. 2014 Jan 31;12(1):12.

47. Abramovich D, Rodriguez Celin A, Hernandez F, Tesone M, Parborell F. Spatiotemporal analysis of the protein expression of angiogenic factors and their related receptors during folliculogenesis in rats with and without hormonal treatment. J Reprod Fertil. 2009 Feb;137(2):309–20.

48. Kiriakidou M, McAllister JM, Sugawara T, Strauss JF 3rd. Expression of steroidogenic acute regulatory protein (StAR) in the human ovary. J Clin Endocrinol Metab. 1996 Nov;81(11):4122–8.

49. Yamamoto S, Konishi I, Tsuruta Y, Nanbu K, Mandai M, Kuroda H, et al. Expression of vascular endothelial growth factor (VEGF) during folliculogenesis and corpus luteum formation in the human ovary. Gynecol Endocrinol. 1997 Dec;11(6):371–81.

50. Estienne A, Relav L, Benkoura M, Monniaux D, Morin F, Fabre S, et al. Endothelial cell-derived fibroblast growth factor-18 regulates ovarian function in sheep. J Cell Physiol. 2022 May;237(5):2528–38.

51. Chai C, Liang L, Mikkelsen NS, Wang W, Zhao W, Sun C, et al. Single-cell transcriptome analysis of epithelial, immune, and stromal signatures and interactions in human ovarian cancer. Commun Biol. 2024 Jan 26;7(1):131.

52. Bayly-Jones C, Pang SS, Spicer BA, Whisstock JC, Dunstone MA. Ancient but not forgotten: New insights into MPEG1, a macrophage perforin-like immune effector. Front Immunol. 2020 Oct 15;11:581906.

53. Bülow S, Zeller L, Werner M, Toelge M, Holzinger J, Entzian C, et al. Bactericidal/permeability-increasing protein is an enhancer of bacterial lipoprotein recognition. Front Immunol. 2018 Dec 5;9:2768.

54. Baldwin LA, Hoff JT, Lefringhouse J, Zhang M, Jia C, Liu Z, et al. CD151-α3β1 integrin complexes suppress ovarian tumor growth by repressing slug-mediated EMT and canonical Wnt signaling. Oncotarget. 2014 Dec 15;5(23):12203–17.

55. Wood NJ, Mattiello T, Rowe ML, Ward L, Perillo M, Arnone MI, et al. Neuropeptidergic systems in Pluteus larvae of the sea urchin Strongylocentrotus purpuratus: Neurochemical complexity in a “simple” nervous system. Front Endocrinol (Lausanne). 2018 Oct 25;9:628.

56. Pagowski V. A description of the bat star nervous system throughout larval ontogeny. Evol Dev. 2024 Jan;26(1):e12468.

57. Kee K, Angeles VT, Flores M, Nguyen HN, Reijo Pera RA. Human DAZL, DAZ and

949 BOULE genes modulate primordial germ-cell and haploid gamete formation.
950 Nature. 2009 Nov 12;462(7270):222–5.

951 58. Gonzalez LE, Tang X, Lin H. Maternal Piwi regulates primordial germ cell
952 development to ensure the fertility of female progeny in Drosophila. Genetics. 2021
953 Aug 26;219(1).

954 59. McCarthy A, Sarkar K, Martin ET, Upadhyay M, Jang S, Williams ND, et al. Msl3
955 promotes germline stem cell differentiation in female Drosophila. Development.
956 2022 Jan 1;149(1).

957 60. Sage J, Martin L, Meuwissen R, Heyting C, Cuzin F, Rassoulzadegan M. Temporal
958 and spatial control of the Sycp1 gene transcription in the mouse meiosis: regulatory
959 elements active in the male are not sufficient for expression in the female gonad.
960 Mech Dev. 1999 Jan;80(1):29–39.

961 61. Hu W, Gauthier L, Baibakov B, Jimenez-Movilla M, Dean J. FIGLA, a basic helix-
962 loop-helix transcription factor, balances sexually dimorphic gene expression in
963 postnatal oocytes. Mol Cell Biol. 2010 Jul;30(14):3661–71.

964 62. Raz E. The function and regulation of vasa-like genes in germ-cell development.
965 Genome Biol. 2000 Sep 1;1(3):REVIEWS1017.

966 63. Campolo F, Gori M, Favaro R, Nicolis S, Pellegrini M, Botti F, et al. Essential role of
967 Sox2 for the establishment and maintenance of the germ cell line. Stem Cells. 2013
968 Jul;31(7):1408–21.

969 64. Moore FL, Jaruzelska J, Fox MS, Urano J, Firpo MT, Turek PJ, et al. Human
970 Pumilio-2 is expressed in embryonic stem cells and germ cells and interacts with
971 DAZ (Deleted in AZoospermia) and DAZ-like proteins. Proc Natl Acad Sci U S A.
972 2003 Jan 21;100(2):538–43.

973 65. Nilsson EE, Doraiswamy V, Skinner MK. Transforming growth factor-beta isoform
974 expression during bovine ovarian antral follicle development. Mol Reprod Dev.
975 2003 Nov;66(3):237–46.

976 66. Zarate-Garcia L, Lane SIR, Merriman JA, Jones KT. FACS-sorted putative oogonial
977 stem cells from the ovary are neither DDX4-positive nor germ cells. Sci Rep. 2016
978 Jun 15;6(1):27991.

979 67. Huyhn K, Renfree MB, Graves JA, Pask AJ. ATRX has a critical and conserved
980 role in mammalian sexual differentiation. BMC Dev Biol. 2011 Jun 14;11(1):39.

981 68. Yu C, Fan X, Sha QQ, Wang HH, Li BT, Dai XX, et al. CFP1 regulates histone
982 H3K4 trimethylation and developmental potential in mouse oocytes. Cell Rep. 2017
983 Aug 1;20(5):1161–72.

984 69. Jiang Y, Zhang HY, Lin Z, Zhu YZ, Yu C, Sha QQ, et al. CXXC finger protein 1-

985 mediated histone H3 lysine-4 trimethylation is essential for proper meiotic
986 crossover formation in mice. Development. 2020 Mar 17;147(6):dev183764.

987 70. Moreno SG, Attali M, Allemand I, Messiaen S, Fouchet P, Coffigny H, et al.
988 TGFbeta signaling in male germ cells regulates gonocyte quiescence and fertility in
989 mice. Dev Biol. 2010 Jun 1;342(1):74–84.

990 71. Belli M, Shimasaki S. Molecular aspects and clinical relevance of GDF9 and
991 BMP15 in ovarian function. Vitam Horm. 2018;107:317–48.

992 72. D'Aniello E, Paganos P, Anishchenko E, D'Aniello S, Arnone MI. Comparative
993 Neurobiology of Biogenic Amines in Animal Models in Deuterostomes. Front Ecol
994 Evol. 2020 Sep 25;8.

995 73. Bhat US, Shahi N, Surendran S, Babu K. Neuropeptides and behaviors: How small
996 peptides regulate nervous system function and behavioral outputs. Front Mol
997 Neurosci. 2021 Dec 2;14:786471.

998 74. Tian S, Zandawala M, Beets I, Baytemur E, Slade SE, Scrivens JH, et al.
999 Urbilaterian origin of paralogous GnRH and corazonin neuropeptide signalling
1000 pathways. Sci Rep. 2016 Jun 28;6:28788.

1001 75. Yañez-Guerra LA, Zhong X, Moghul I, Butts T, Zampronio CG, Jones AM, et al.
1002 Echinoderms provide missing link in the evolution of PrRP/sNPF-type neuropeptide
1003 signalling. Elife. 2020 Jun 24;9.

1004 76. Escudero Castelán N, Semmens DC, Guerra LAY, Zandawala M, Dos Reis M,
1005 Slade SE, et al. Receptor deorphanization in an echinoderm reveals kisspeptin
1006 evolution and relationship with SALMFamide neuropeptides. BMC Biol. 2022 Aug
1007 24;20(1):187.

1008 77. Yañez-Guerra LA, Delroisse J, Barreiro-Iglesias A, Slade SE, Scrivens JH, Elphick
1009 MR. Discovery and functional characterisation of a luqin-type neuropeptide
1010 signalling system in a deuterostome. Sci Rep. 2018 May 8;8(1):7220.

1011 78. Odekunle EA, Semmens DC, Martynyuk N, Tinoco AB, Garewal AK, Patel RR, et
1012 al. Ancient role of vasopressin/oxytocin-type neuropeptides as regulators of feeding
1013 revealed in an echinoderm. BMC Biol. 2019 Jul 31;17(1):60.

1014 79. Semmens DC, Dane RE, Pancholi MR, Slade SE, Scrivens JH, Elphick MR.
1015 Discovery of a novel neurophysin-associated neuropeptide that triggers cardiac
1016 stomach contraction and retraction in starfish. J Exp Biol. 2013 Nov 1;216(Pt
1017 21):4047–53.

1018 80. Perillo M, Arnone MI. Characterization of insulin-like peptides (ILPs) in the sea
1019 urchin Strongylocentrotus purpuratus: insights on the evolution of the insulin family.
1020 Gen Comp Endocrinol. 2014 Sep 1;205:68–79.

1021 81. Acevedo-Rodriguez A, Kauffman AS, Cherrington BD, Borges CS, Roepke TA,
1022 Laconi M. Emerging insights into hypothalamic-pituitary-gonadal axis regulation
1023 and interaction with stress signalling. J Neuroendocrinol. 2018 Oct;30(10):e12590.

1024 82. Szukiewicz D. Current insights in prolactin signaling and ovulatory function. Int J
1025 Mol Sci. 2024 Feb 6;25(4):1976.

1026 83. Clay CM, Cherrington BD, Navratil AM. Plasticity of anterior pituitary gonadotrope
1027 cells facilitates the pre-ovulatory LH surge. Front Endocrinol (Lausanne).
1028 2020;11:616053.

1029 84. Albertini D, Bromfield J. Soma-Germline Interactions in the Ovary: An Evolutionary
1030 Perspective. In: Oogenesis. Chichester, UK: John Wiley & Sons, Ltd; 2010. p. 103–
1031 13.

1032 85. Wu Z, Yang L, He Q, Zhou S. Regulatory mechanisms of vitellogenesis in insects.
1033 Front Cell Dev Biol. 2020;8:593613.

1034 86. Liu W, Xin Q, Wang X, Wang S, Wang H, Zhang W, et al. Estrogen receptors in
1035 granulosa cells govern meiotic resumption of pre-ovulatory oocytes in mammals.
1036 Cell Death Dis. 2017 Mar 9;8(3):e2662–e2662.

1037 87. Planas JV, Athos J, Goetz FW, Swanson P. Regulation of ovarian steroidogenesis
1038 in vitro by follicle-stimulating hormone and luteinizing hormone during sexual
1039 maturation in Salmonid Fish1. Biol Reprod. 2000 May 1;62(5):1262–9.

1040 88. Shirai H, Kanatani H, Taguchi S. 1-methyladenine biosynthesis in starfish ovary:
1041 action of gonad-stimulating hormone in methylation. Science. 1972 Mar
1042 24;175(4028):1366–8.

1043 89. Kanatani H, Shirai H, Nakanishi K, Kurokawa T. Isolation and identification of
1044 meiosis inducing substance in starfish Asterias amurensis. Nature. 1969
1045 Jan;221(5177):273–4.

1046 90. Johnson ET, Nicola T, Roarty K, Yoder BK, Haycraft CJ, Serra R. Role for primary
1047 cilia in the regulation of mouse ovarian function. Dev Dyn. 2008 Aug;237(8):2053–
1048 60.

1049 91. Trombly DJ, Woodruff TK, Mayo KE. Roles for transforming growth factor beta
1050 superfamily proteins in early folliculogenesis. Semin Reprod Med. 2009
1051 Jan;27(1):14–23.

1052 92. Kipp JL, Golebiowski A, Rodriguez G, Demczuk M, Kilen SM, Mayo KE. Gene
1053 expression profiling reveals Cyp26b1 to be an activin regulated gene involved in
1054 ovarian granulosa cell proliferation. Endocrinology. 2011 Jan;152(1):303–12.

1055 93. Ivarsson K, Sundfeldt K, Brännström M, Janson PO. Production of steroids by
1056 human ovarian surface epithelial cells in culture: possible role of progesterone as

1057 growth inhibitor. Gynecol Oncol. 2001 Jul;82(1):116–21.

1058 94. Kloc M, Tworzydło W, Szklarzewicz T. Germline and somatic cell syncytia in
1059 insects. Results Probl Cell Differ. 2024;71:47–63.

1060 95. Tingen C, Kim A, Woodruff TK. The primordial pool of follicles and nest breakdown
1061 in mammalian ovaries. Mol Hum Reprod. 2009 Dec;15(12):795–803.

1062 96. Roco ÁS, Ruiz-García A, Bullejos M. Testis development and differentiation in
1063 amphibians. Genes (Basel). 2021 Apr 16;12(4):578.

1064 97. Smaga CR, Bock SL, Johnson JM, Parrott BB. Sex determination and ovarian
1065 development in reptiles and amphibians: From genetic pathways to environmental
1066 influences. Sex Dev. 2023;17(2-3):99–119.

1067 98. Hall GB, Long JA, Wood BJ, Bedecarrats GY. Germ cell dynamics during nest
1068 breakdown and formation of the primordial follicle pool in the domestic turkey
1069 (Meleagris gallopavo). Poult Sci. 2020 May;99(5):2746–56.

1070 99. Spradling AC, Niu W, Yin Q, Pathak M, Maurya B. Conservation of oocyte
1071 development in germline cysts from Drosophila to mouse. Elife. 2022 Nov 29;11.

1072 100. Wang Z, Liu CY, Zhao Y, Dean J. FIGLA, LHX8 and SOHLH1 transcription factor
1073 networks regulate mouse oocyte growth and differentiation. Nucleic Acids Res.
1074 2020 Apr 17;48(7):3525–41.

1075 101. De La Fuente R, Viveiros MM, Wigglesworth K, Eppig JJ. ATRX, a member of the
1076 SNF2 family of helicase/ATPases, is required for chromosome alignment and
1077 meiotic spindle organization in metaphase II stage mouse oocytes. Dev Biol. 2004
1078 Aug 1;272(1):1–14.

1079 102. Lesch BJ, Page DC. Genetics of germ cell development. Nat Rev Genet. 2012
1080 Nov;13(11):781–94.

1081 103. Nicholls PK, Schorle H, Naqvi S, Hu YC, Fan Y, Carmell MA, et al. Mammalian
1082 germ cells are determined after PGC colonization of the nascent gonad. Proc Natl
1083 Acad Sci U S A. 2019 Dec 17;116(51):25677–87.

1084 104. Hickford DE, Frankenberg S, Pask AJ, Shaw G, Renfree MB. DDX4 (VASA) is
1085 conserved in germ cell development in marsupials and monotremes. Biol Reprod.
1086 2011 Oct;85(4):733–43.

1087 105. Hartung O, Forbes MM, Marlow FL. Erratum: Zebrafish vasa is required for germ-
1088 cell differentiation and maintenance. Mol Reprod Dev. 2016 Dec;83(12):1128–30.

1089 106. Chen Y, Lin X, Dai J, Bai Y, Liu F, Luo D. Deletion of ddx4 ovary-specific transcript
1090 causes dysfunction of meiosis and derepress of DNA transposons in zebrafish
1091 ovaries. Biology (Basel). 2024 Dec 16;13(12).

1092 107. Liu N, Han H, Lasko P. Vasa promotes *Drosophila* germline stem cell differentiation
1093 by activating *mei-P26* translation by directly interacting with a (U)-rich motif in its 3′
1094 UTR. Genes Dev. 2009 Dec 1;23(23):2742–52.

1095 108. Bristol-Gould SK, Kreeger PK, Selkirk CG, Kilen SM, Cook RW, Kipp JL, et al.
1096 Postnatal regulation of germ cells by activin: the establishment of the initial follicle
1097 pool. Dev Biol. 2006 Oct 1;298(1):132–48.

1098 109. Iang Y. Hedgehog pathway inhibition causes primary follicle atresia and decreases
1099 female germline stem cell proliferation capacity or stemness. Stem Cell Res Ther.
1100 2019;10.

1101 110. Le Rolle M, Massa F, Siggers P, Turchi L, Loubat A, Koo BK, et al. Arrest of
1102 WNT/β-catenin signaling enables the transition from pluripotent to differentiated
1103 germ cells in mouse ovaries. Proc Natl Acad Sci U S A. 2021 Jul
1104 27;118(30):e2023376118.

1105 111. Zhang X, Gunewardena S, Wang N. Nutrient restriction synergizes with retinoic
1106 acid to induce mammalian meiotic initiation in vitro. Nat Commun. 2021 Mar
1107 19;12(1):1758.

1108 112. Moguilevsky JA, Wuttke W. Changes in the control of gonadotrophin secretion by
1109 neurotransmitters during sexual development in rats. Exp Clin Endocrinol Diabetes.
1110 2001;109(4):188–95.

1111 113. Liu X, Herbison AE. Dopamine regulation of gonadotropin-releasing hormone
1112 neuron excitability in male and female mice. Endocrinology. 2013 Jan;154(1):340–
1113 50.

1114 114. Camille Melón L, Maguire J. GABAergic regulation of the HPA and HPG axes and
1115 the impact of stress on reproductive function. J Steroid Biochem Mol Biol. 2016
1116 Jun;160:196–203.

1117 115. Kaiser UB. Hyperprolactinemia and infertility: new insights. J Clin Invest. 2012
1118 Oct;122(10):3467–8.

1119 116. Xie Q, Kang Y, Zhang C, Xie Y, Wang C, Liu J, et al. The role of kisspeptin in the
1120 control of the hypothalamic-pituitary-gonadal axis and reproduction. Front
1121 Endocrinol (Lausanne). 2022 Jun 28;13:925206.

1122 117. A.B. Chaet and R.A. McConnaughy. Physiologic Activity of Nerve Extracts. The
1123 Biological Bulletin. 1959;117:407–8.

1124 118. Feng Y, Piñon Gonzalez VM, Lin M, Egertová M, Mita M, Elphick MR. Localization
1125 of relaxin-like gonad-stimulating peptide expression in starfish reveals the
1126 gonoducts as a source for its role as a regulator of spawning. J Comp Neurol. 2023
1127 Sep;531(13):1299–316.

1128 119. Chaiyamoon A, Tinikul R, Nontunha N, Chaichotranunt S, Poomtong T, Sobhon P,
1129 et al. Characterization of TRH/GnRH-like peptides in the sea cucumber, Holothuria
1130 scabra, and their effects on oocyte maturation. Aquaculture. 2020
1131 Mar;518(734814):734814.

Supplementary Figures

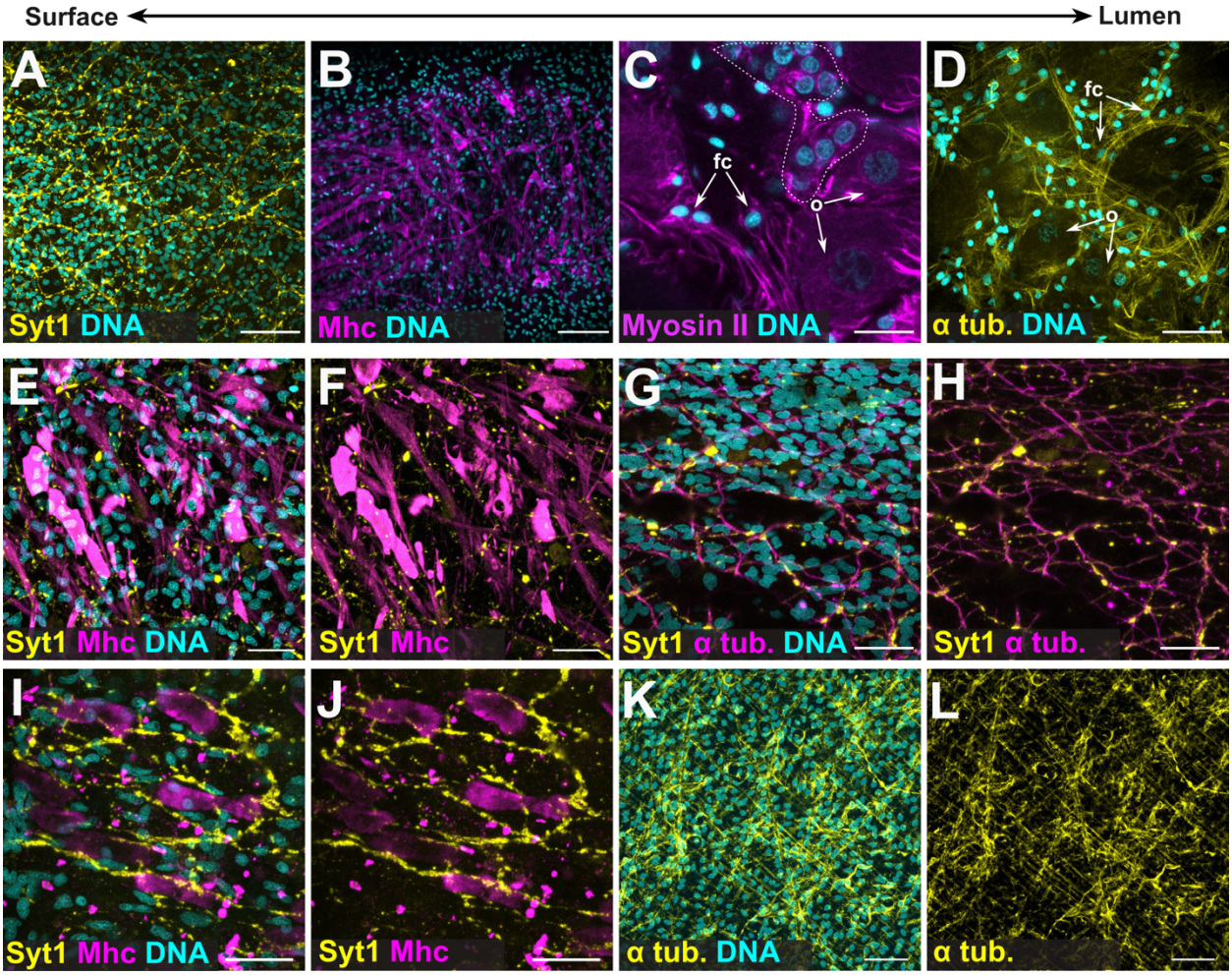

Figure S1. Immunohistochemical identification of echinoderm ovarian cell types. (A-D) IHC for Syt1 labeling neurons (A), for Mhc labeling muscles (B) and for myosin (C) and α-tubulin (D) labeling follicle cells. Scale bars for panels A and D are 40 µm; for panel B 60 µm; for C 20 µm. **(E-F)** IHC for Syt1 and Mhc to visualize the interconnection of ovarian neurons and muscles. Scale bars for panels are 20 µm. **(G-H)** IHC for Syt1 and α-tubulin co-labels the ovarian neurons. Scale bars for panels are 20 µm. **(I-J)** IHC for Syt1 and Mhc confirms the presence of the neurons and muscles respectively in the sea urchin *S. purpuratus* ovary. Scale bars are 25 µm. **(K-L)** IHC for α tubulin labels the ovarian neurons in the sea cucumber *H. tubulosa* ovary. Scale bars are 50 µm. Nuclei were labelled with DAPI (cyan). fc, follicle cells; o, oocytes.

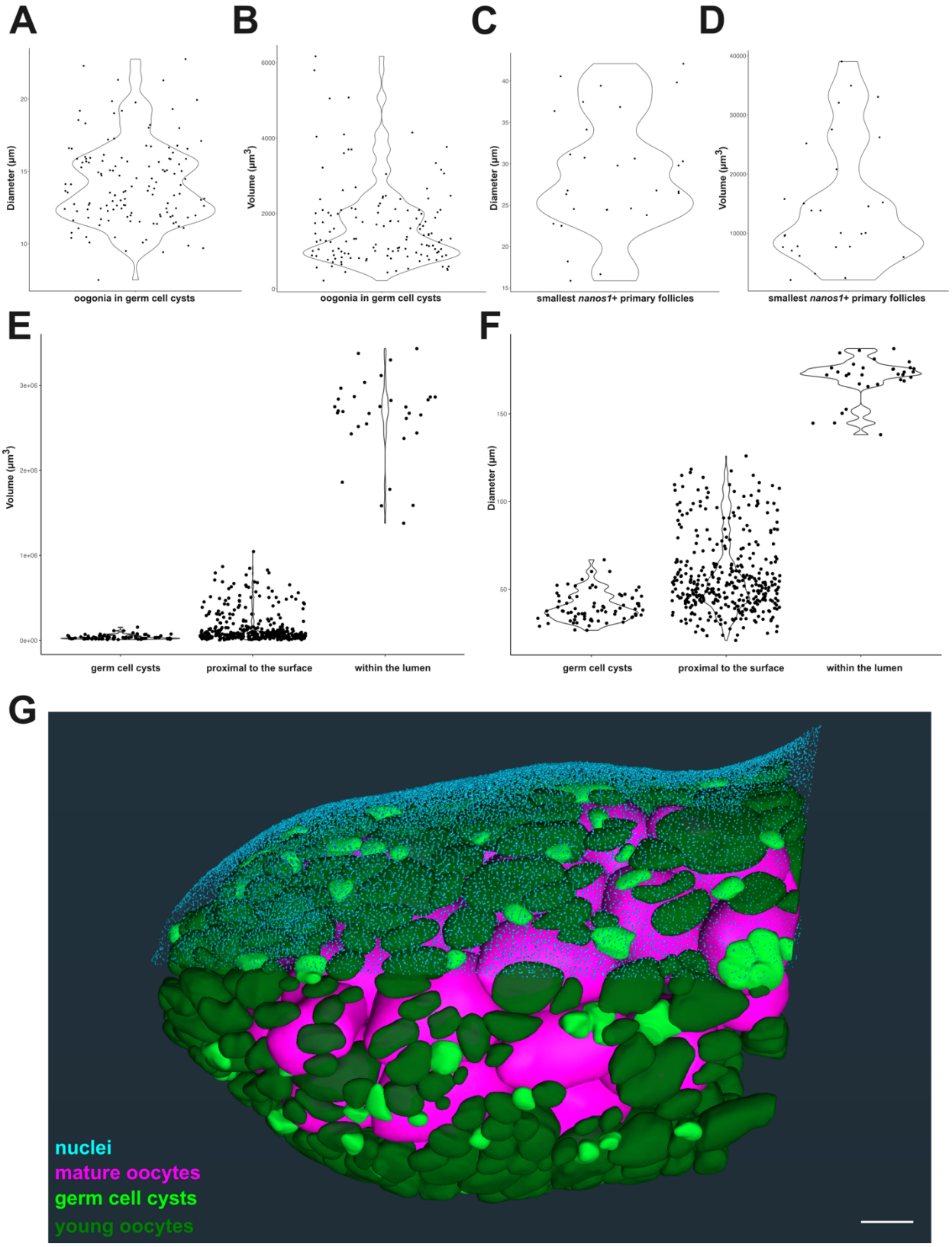
A
B
C
D
Diameter (µm)
Volume (µm3)
oogonia in germ cell cysts
oogonia in germ cell cysts
smallest nanos1+ primary follicles
smallest nanos1+ primary follicles
E
F
Volume (µm3)
Diameter (µm)
germ cell cysts
proximal to the surface
within the lumen
germ cell cysts
proximal to the surface
within the lumen
G
nuclei
mature oocytes
germ cell cysts
young oocytes

1143

1144 **Figure S2. Size and spatial distributions of oogonia and oocytes in the sea star ovary. (A-B)** Violin
1145 plot showing the experimentally measured diameter (A) and estimated volume (B) of each oogonium within
1146 germ cell cysts. **(C-D)** Violin plot showing the measured diameter (C) and estimated volume (D) of the
1147 smallest *nanos1* positive oocyte in close proximity to the germ cell cysts. **(E-F)** Violin plot of the
1148 segmentation-based calculated volumes (E) and estimated diameter (F) of germ cell cysts, oocytes close
1149 to the ovarian surface, and those within the lumen. **(G)** 3D rendering of segmented germ cell cysts and
1150 oocytes. Scale bar is 100 µm. Ovary seen from a side view. Estimated volumes or diameters were
1151 calculated based on experimentally measured diameters or volumes respectively, assuming the shape of
1152 the oogonia and oocytes is spherical.

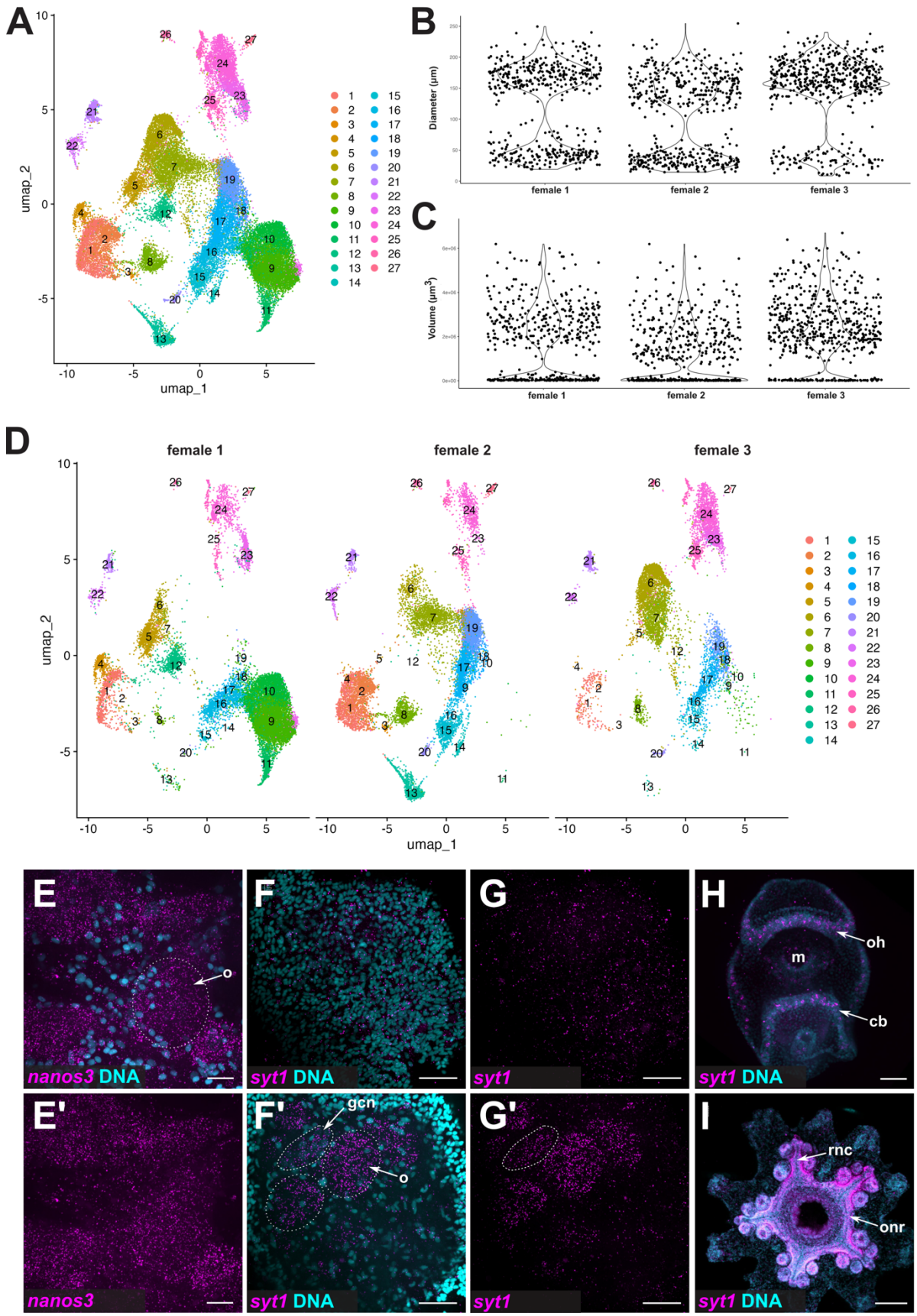
A
umap_1
umap_2
B
Diameter (µm)
female 1
female 2
female 3
C
Volume (µm³)
female 1
female 2
female 3
D
female 1
female 2
female 3
umap_1
umap_2
E
o
nanos3 DNA
F
syt1 DNA
G
syt1
H
oh
m
cb
syt1 DNA
E'
nanos3
F'
gcn
o
syt1 DNA
G'
syt1
I
rnc
onr
syt1 DNA

1153

1154 **Figure S3. *P. miniata* ovary cell atlas and cell contribution of the different libraries. (A)** Integrated
1155 UMAP of the three different scRNA-seq libraries, in which color code is indicative of different clusters **(B-**
1156 **C)** Violin plot showing the experimentally measured diameter (B) and estimated volume (C) of the oogonia
1157 and oocytes within the ovaries used for the reconstruction of the single cell atlas. Due to the capturing
1158 system limitations only the oocytes with a size ≤ 40µm in diameter are included in the single cell atlas. **(D)**
1159 Integrated UMAP of the three different scRNA-seq libraries, split by the cell contribution of each library. The
1160 color code is indicative of different clusters. **(E-E')** HCR for the *nanos3* gene with (E) and without (E') the
1161 nuclei channel (DAPI) confirmed its localization in the germ lineage. Dotted circles in panel E are indicative
1162 of oocytes. Scale bars are 20 µm. **(F-G')** HCR for the *syt1* gene with (F-F') and without (G-G') the nuclei
1163 channel (DAPI) shows expression in the neurons (F-G) as well as the germ cell cysts and oocytes (F'-G').
1164 Dotted circles in F' are indicative of oocytes. Germ cell cysts in panels F' and G' are outlined with dotted
1165 lines. Scale bars are 20 µm. **(H-I) HCR** for the *syt1* gene with (G) and without (G') the nuclei channel (DAPI)
1166 shows expression of the gene only in the nervous system of the *P. miniata* larvae (H) and post-metamorphic
1167 juveniles (I), confirming the specificity of the probe. Scale bars for panels H and I are 50 and 100 µm
1168 respectively. cb, ciliary band; m, mouth, oocytes; oh, oral hood; onr, oral nerve ring; rnc, radial nerve cord.

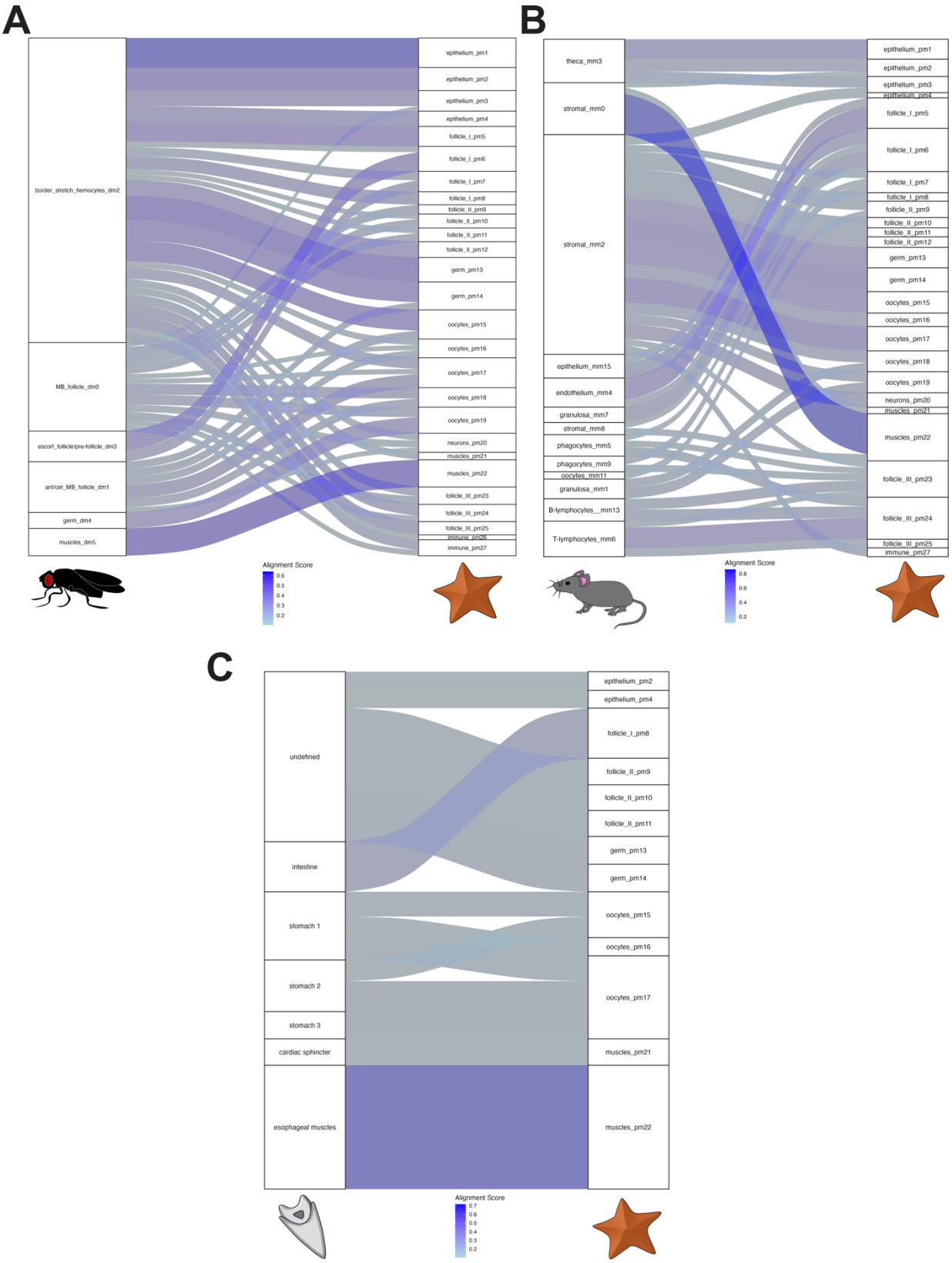

Figure S4. Cross-species comparison of sea star ovarian cell types with protostome and deuterostome representatives with SAMap. Sankey plot depicting the alignment scores between adult

sea star ovarian cell atlas with the adult fruit fly ovary **(A)**, adult mouse ovary **(B)** and with sea urchin larva **(C)**. Alignment scores equal or greater to 0.1 were considered significant.

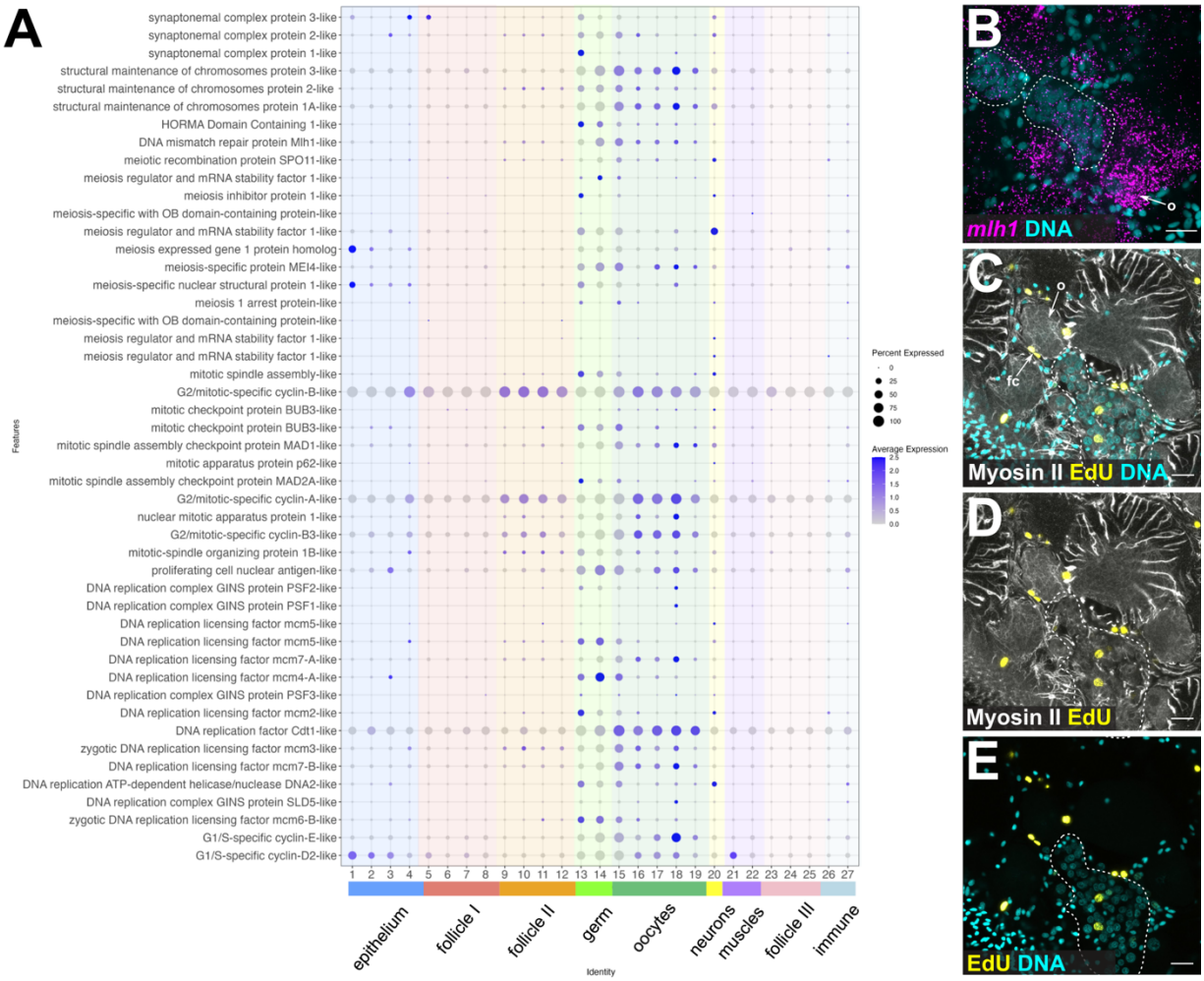

Figure S5. Identification of mitotic and meiotic molecular signatures in the sea star ovary. (A) Dotplot showing the average expression of the genes used for the scoring analysis shown in Fig.4 A. **(B)** HCR for the meiotic marker *mlh1* labelling the germ cell cysts and oocytes of various sizes. **(C-E)** IHC for Myosin II labeling cell peripheries with the EdU proliferation assay, confirms that cells from both the somatic and germ lineages are actively proliferating in the adult sea star ovary. Nuclei are labelled with DAPI (cyan). Dotted lines outline the germ cell cyst in panels C-E. Scale bars are 20 µm. fc, follicle cells; o, oocytes.

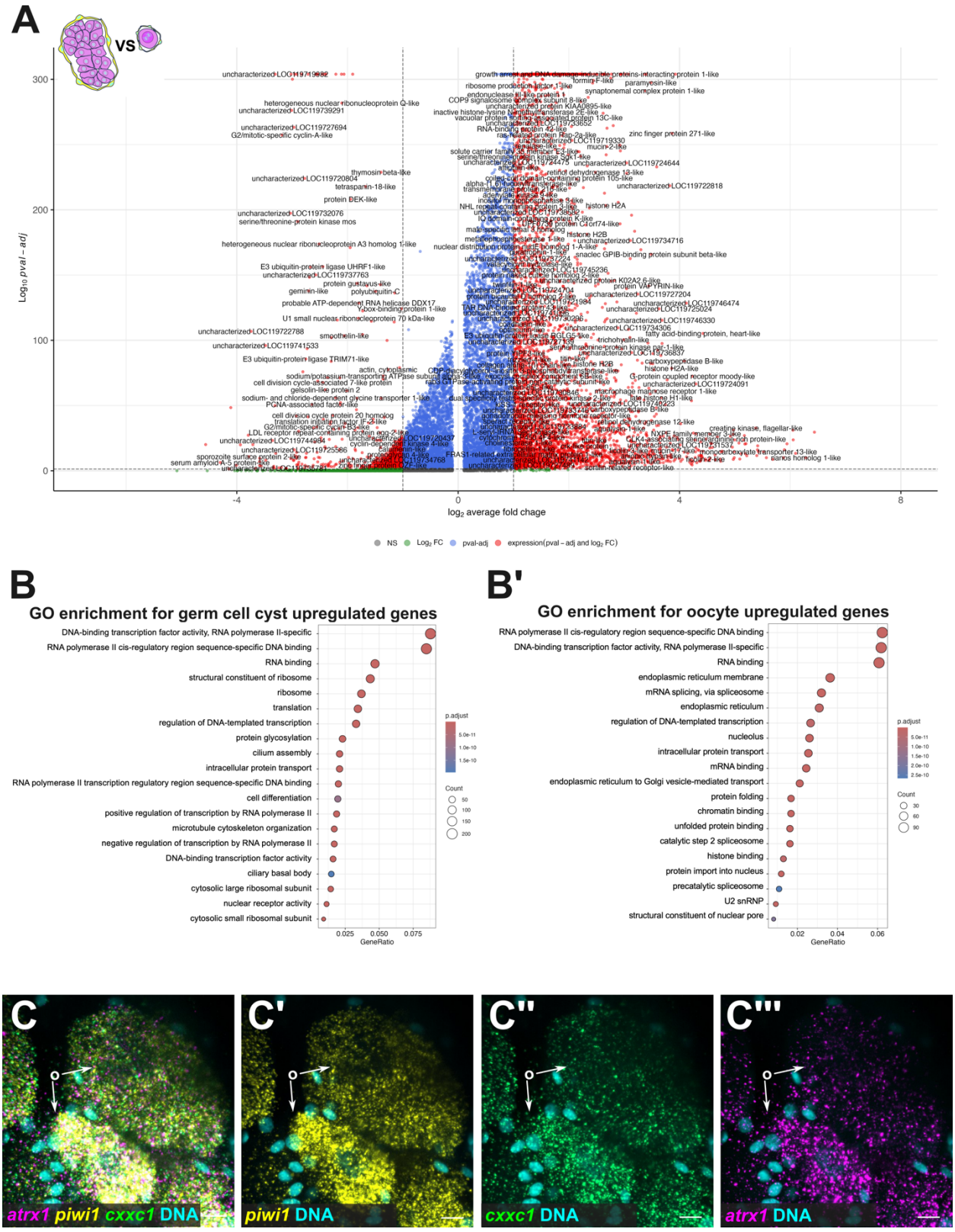

Figure S6. Differential expression patterns along the sea star oogenesis developmental trajectory. **(A)** Volcano plot showing the differential expression of the germ cell cyst (clusters 13 and 14) genes versus

the oocyte reference group (clusters 15-19). **(B-B')** Dotplot showing the top 20 enriched gene ontology terms associated with the germ cell cyst (B) and the oocyte (B') upregulated genes. **(C-C''')** HCR for the transcriptional regulators *atrx1* and *cxxc1* paired with *piwi1* shows expression in oocytes. Scale bars are 10 µm.

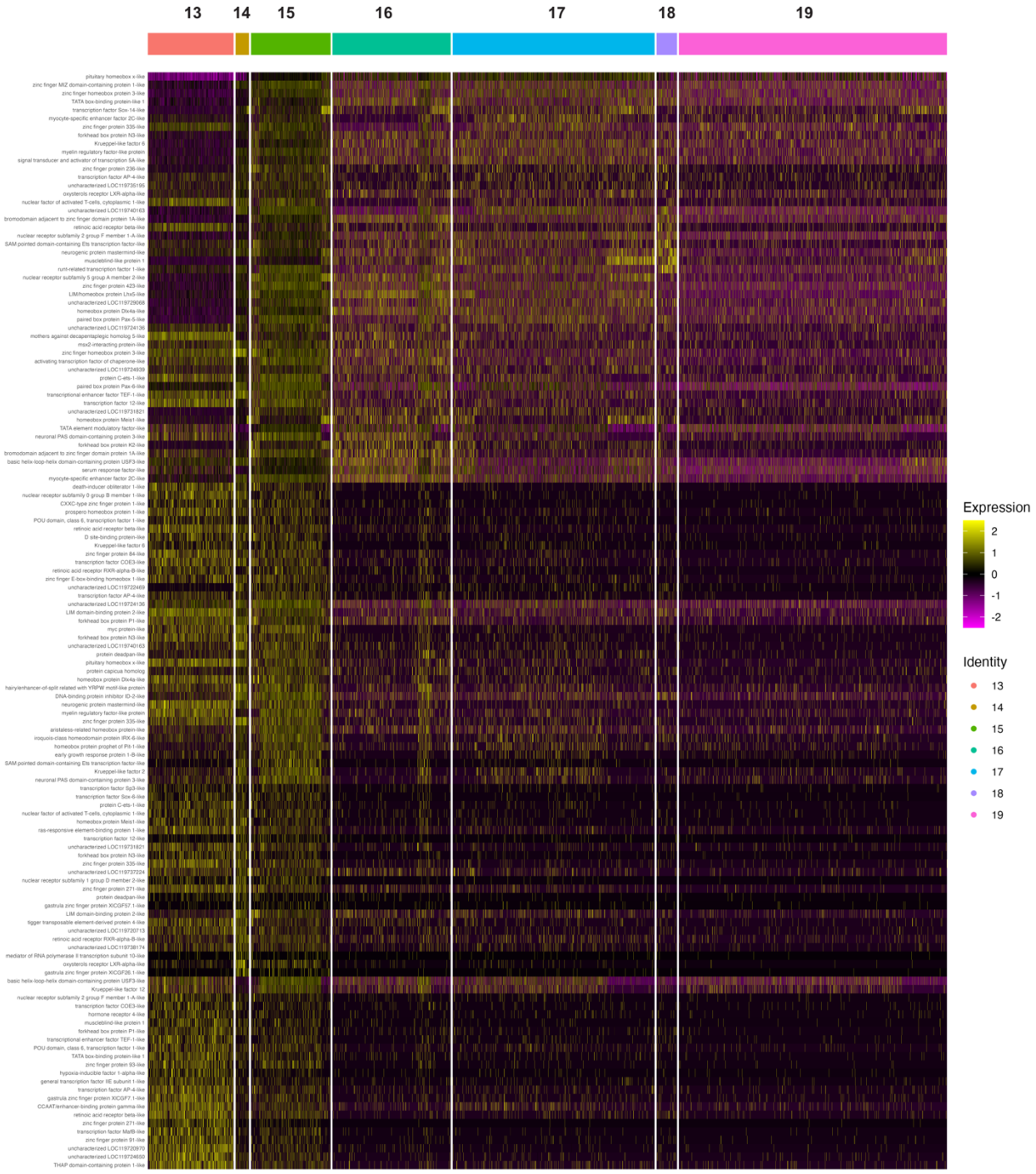

Figure S7. Distinct transcription factor profiles during early oogenesis. Heatmap of the top 50 differentially expressed transcription factors across the germline clusters.

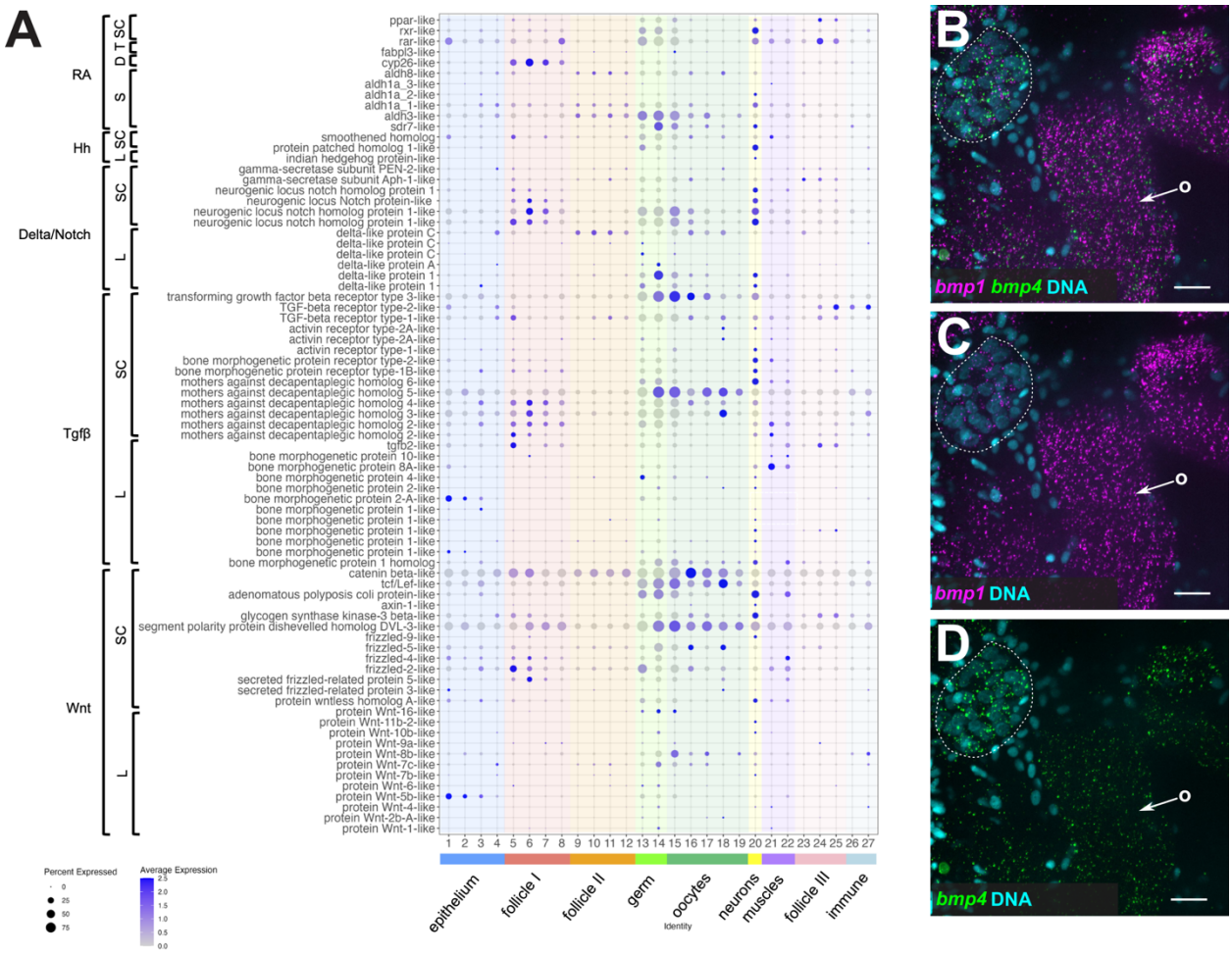

Figure S8. Expression patterns of evolutionarily conserved ovarian signaling pathways. (A) Dotplot showing the average expression of the genes used for the scoring analysis shown in Fig. 6A. D, degradation; L, ligand; S, synthesis; SC, signaling cascade; T, transport. **(B-D)** HCR for the *bmp1* and *bmp4* ligands confirms their spatial expression in the germ cell cysts and oocytes. Nuclei are labelled with DAPI (cyan). Dotted lines outline the germ cell cyst. Scale bars are 20 µm. o, oocytes.

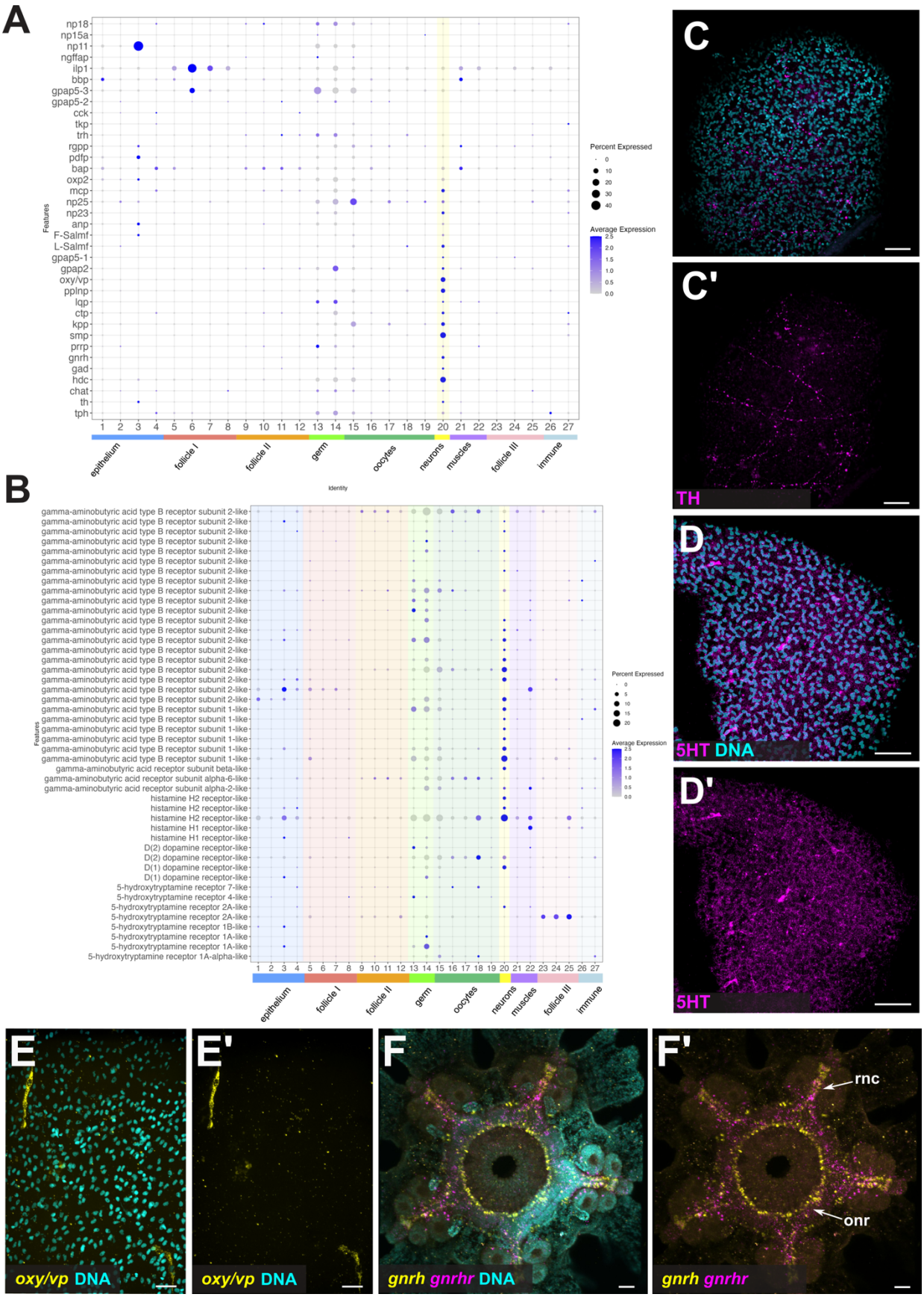
A
B
C
C'
D
D'
E
E'
F
F'
Features
Identity
Percent Expressed
Average Expression
epithelium
follicle I
follicle II
germ
oocytes
neurons
muscles
follicle III
immune
TH
5HT DNA
5HT
oxy/vp DNA
gnrh gnrhr DNA
gnrh gnrhr
rnc
onr

1202

1203 **Figure S9. Neuropeptides and neurotransmitters expressed in the intrinsic ovarian nervous system.**
1204 **(A)** Dotplot showing the average expression of known echinoderm neurotransmitter synthesizing enzymes
1205 and neuropeptides. **(B)** Dotplot showing the average expression of sea star neurotransmitter receptors. **(C-**
1206 **C')** Immunofluorescence of TH shows the presence of subepidermal ovarian dopaminergic neurons. Scale
1207 bars are 40 µm. **(D-D')** Immunofluorescence of 5HT confirms the presence of subepidermal ovarian
1208 serotonergic neurons. Scale bars are 40 µm. **(E-E')** HCR for *oxy/vp* neuropeptide marks two *oxy/vp* positive
1209 neurons per ovarian lobe. Scale bars are 20 µm. **(F-F')** HCR for *gnrh* and *gnrhr* shows expression in the
1210 post-metamorphic *P. miniata* nervous system confirming the specificity of the probes. Scale bars are 50
1211 µm. onr, oral nerve ring; rnc, radial nerve cord.